PAPER NAME

Gama Ray Bursts.pdf

AUTHOR

Swetha Gopinathan

WORD COUNT

14064 Words

CHARACTER COUNT

69361 Characters

PAGE COUNT

46 Pages

FILE SIZE

3.3MB

SUBMISSION DATE

Jul 31, 2023 2:16 PM GMT+5:30

REPORT DATE

Jul 31, 2023 2:17 PM GMT+5:30

9% Overall Similarity

The combined total of all matches, including overlapping sources, for each database.

- 7% Internet database
- 7% Publications database
- Crossref database
- Crossref Posted Content database
- 5% Submitted Works database

Excluded from Similarity Report

- Bibliographic material
- Quoted material
- Cited material
- Small Matches (Less then 12 words)
- Manually excluded text blocks

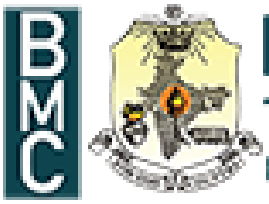

BHARATA MATA COLLEGE
THRIKKAKARA. KERALA 682021
Re-accredited by NAAC with 'A+' Grade | ISO 9001-2015 Certified

DEPARTMENT OF PHYSICS

ANALYSIS OF GAMMA-RAY BURSTS USING FAST FOURIER TRANSFORM

PROJECT REPORT

Submitted by,

Swetha Gopinathan 210011023202

Under the guidance of

Dr. Manesh Michael
Assistant Professor, Department of Physics,
Bharata Mata College, Thrikkakara
Visiting Associate, IUCAA, Pune

Dr. Amit Shukla
Assistant Professor, DAASE,
Indian Institute of Technology,
Indore

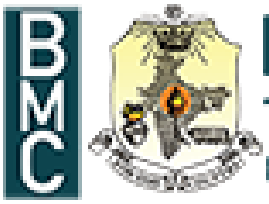

BHARATA MATA COLLEGE
THRIKKAKARA. KERALA 682021
Re-accredited by NAAC with 'A+' Grade | ISO 9001-2015 Certified

DEPARTMENT OF PHYSICS

CERTIFICATE

This is the certification for the project work named as "Analysis of Gamma-Ray Bursts using Fast Fourier Transform" carried out by Ms. Swetha Gopinathan (210011023202), who is bonafide student of Bharata Mata College, Thrikkakara in partial fulfilment for the award of Degree of Master of Science in Space Science of Mahatma Gandhi University, Kottayam, in the academic year 2021-2023. It is authorized that all corrections indicated for Internal Assessment have been embodied in the report, handed over to the departmental library. The project report has been accepted as it complies with the academic requirements in respect of project work recommended by the institution for the forenamed Degree.

Signature of Internal Guide
Dr. Manesh Michael

Signature of External Guide
Dr. Amit Shukla

Signature of HoD
Dr. Shibi Thomas

Signature of Principal
Dr.Johnson K M

भारतीय प्रौद्योगिकी संस्थान इंदौर
सिमरोल, इंदौर 453 552, भारत

Indian Institute of Technology Indore
Simrol, Indore 453 552, India

Office: +91 731243 8700
Extn : 3213

IIT Indore

From
Dr. Amit Shukla, Assistant Professor
Department of Astronomy, Astrophysics and Space Engineering
Indian Institute of Technology Indore
Simrol, Indore - 453552, India
Webpage: https://sites.google.com/iiti.ac.in/welcome/home

Date: July 31 , 2023
E-mail: amit.shukla@iiti.ac.in
Mobile: +91 9579293880

Whom it may concern

This is to certify that **Ms. Swetha Gopinathan** (210011023202), 4th semester M. Sc. Space Science student at **Bharata Mata College, Thrikkakkara, Ernakulam** (Affiliated to Mahatma Gandhi University, Kottayam) has completed her project work in online mode under my supervision during April 2023 to 5 June 2023.

She has worked on the "**Analysis of Gamma-Ray Bursts using Fast Fourier Transform**" project—the project aimed to study variability in the gamma-ray burst (GRBs) using Power Spectral Density (PSD). During the project, her performance was very good. She has developed an analysis pipeline to compute PSD and studied variability at gamma-rays of ten GRBs.

Your sincerely

Dr. Amit Shukla

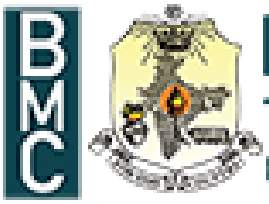

BHARATA MATA COLLEGE
THRIKKAKARA. KERALA 682021
Re-accredited by NAAC with 'A+' Grade | ISO 9001-2015 Certified

DECLARATION

I, Swetha Gopinathan(210011023202), student of fourth semester M.Sc Space Science, Department of Physics, Bharata Mata College, Thrikkakara, hereby declare that the project titled "Analysis of Gamma-Ray Bursts using Fast Fourier Transform" has been implemented by me and submitted in partial fulfilment of fourth semester requirements in Master of Science in Space Science from Mahatma Gandhi University, Kottayam during the academic year 2021-2023.

I also declare that the matter of this dissertation has not been submitted previously by anybody else for the award of any degree or diploma to any other university.

Further I declare that any Intellectual Property Rights created out of this project will be the property of Bharata Mata College, Thrikkakara and I will be one of the authors of the same.

Place: Thrikkakara
Date:

Name Signature

Swetha Gopinathan(210011023202)

ACKNOWLEDGEMENT

The completion and success of this project involves not only an individual but on a group of people whose assistance, aids and guidance, requires a special acknowledgement. Including academic scholars and friends, this group have helped me in achieving the best I could with this project. I would like to express my gratitude towards them.

I extend my earnest gratefulness and honor for being able to work on this project under the guidance of my external project guide, Dr. Amit Shukla, Assistant Professor, Department of Astronomy, Astrophysics and Space Engineering(DAASE) at Indian Institute of Technology, Indore. The amount of inspiration, guidance and cooperation that he put forward was indescribable. My internal project guide Dr. Manesh Michael, Assistant Professor, Bharata Mata College, had also backed and provided assistance throughout this period and I would like to thank him for that.

I would like to thank Dr. Shibi Thomas, Head of the Department, Bharata Mata College, Thrikkakara, for her cooperation and instructions she granted regarding the works of this project.

My deepest gratitude to the PhD Scholars and Masters students, from Indian Institute of Technology, Indore, working under the guidance of my external guide, Dr. Amit Shukla, for helping and for the advices regarding the procedures required for the completion of this project.

I extend my sincere thankfulness to Dr. Johnson K M, The Principal, Bharata Mata College, Thrikkakara, for providing moral support throughout the project duration.

My ardent gratefulness to my parents and all the faculty members of the Department of Physics of Bharata Mata College, Thrikkakara and Indian Institute of Technology, Indore for their constant encouragement and support. Last, but not the least, I must thank my peers and friends who contributed their valuable suggestions for me at full length of the project period.

ABSTRACT

Gamma-ray bursts (GRB) are immensely energetic explosions that occur at several milliseconds to a few minute time scales. GRBs are classified based on the time interval of fluence observed (T_{90} duration) as short and long GRBs. The variations in the gamma rays emitted from the GRBs have been studied using their light curve in this project. The GRB light curves may vary in shape, ranging from continuous single pulses to numerous peaks well isolated in time. The light curves obtained from the GRBs are converted to the frequency domain using Fast Fourier transforms by a Python code. The FFT is used to compute GRB light curves' Power Spectral Density (PSD). These observations enable us to understand underlying processes in the bursts. The information obtained from their light curves provides insights regarding these GRBs' progenitors and host galaxies. The sample of ten GRBs is analyzed to study variability at gamma-ray using data from Fermi-GBM. A power-law function is used to model the slope of PSDs obtained from GRB light curves. The power law's observed slope is consistent with the pink noise process. Our study could not find any significant differences in the variability pattern between the two classes of GRBs. Still, this procedure can be further extended for a larger sample.

Contents

Chapter 1

Introduction

Gamma-Ray Bursts(GRBs) which are brief and energetic pulses of γ-rays having low energy, was discovered in the late sixties accidentally when satellites were launched by the U.S military to detect gamma radiations emitted by nuclear weapons tested in space. Ever since then, astrophysicists and astronomers have always been in search for explanations of this phenomenon. They are the most dynamic outbursts occurring in our universe among the other electromagnetic radiations emitted and are possibly a source of ultra high-energy cosmic rays(Piran 2005; Coppin *et al.* 2020). The studies about GRBs took a rapid transformation in the last decade when space expeditions like Burst and Transient Source Experiment(BATSE) on Compton Gamma-Ray Observatory(CGRO), BeppoSAX and High-Energy Transient Explorer and other ground observatories together showed that GRBs are cosmological, have precursor emissions and long lasting afterglows and are associated with core collapse supernovae and mergers between binary systems(two neutron star systems or a neutron star-black hole systems).

The nature of GRBs that they are highly luminous flashes taking place in a brief amount of time and their origin, radiation mechanisms, the information that they carry about host galaxies and further characteristics all have been of great passion for all physicists of the time of its discovery. The amount of energy that these abrupt explosions releases with such a short span of time(seconds), is even greater compared to the amount of energy that the Sun releases in its lifetime. Such explosions carry with them all sorts of knowledge about their surroundings. Putting together the studies of plotting light curves from the data obtained from the satellites, then finding its Fourier Transform(FT) and Power Density Spectrum(PDS), can reveal many information regarding the GRB. These information include the variation in the photon counts emitted in the burst with time, the frequencies at which emissions occur with their respective intensities, the power-law behaviour exhibited by the GRB light curves and any other deviations from the expected measurements like precursors or noises due to some other reasons.

The γ-ray sources in the sky have been observed since 2008 by the Fermi Gamma-Ray Space Telescope, which was introduced as a mission to do multi-wavelength studies, and covers the entire unocculted sky from a lower Earth orbit. There are two scientific instruments aboard the Space Telescope, the Large Area Telescope(LAT) and the Gamma-Ray Burst Monitor(GBM), together they cover 8 orders of magnitude in photon energy. The LAT covers high energy ranges whereas GBM gives insights to the emissions occurring in

the lower energy range. The large field of view offered by both these instruments enables the observation of the entire sky with measurements for about an hour for GBM and three hours for LAT and soon after that all the data from Fermi will be available for the public. Gamma-Ray Bursts including those associated with neutron star mergers detected in gravitational waves, in a number of 3000 and other high-energy sources like blazars, in a number of 5000, have been detected by the Fermi instruments. A broad range of resources to use the data scientifically in a number of ways are provided by the Fermi Science Support Centre(FSSC)(Thompson & Wilson-Hodge 2022).

The burst data and the Time-Tagged Event(TTE) data provided by the FSSC, from the detectors of GBM, are used to get the raw photon rates and data with highest resolution. These data, after determining the background levels that did not trigger the detectors, are used to get the light curves which are the plot of photon counts against trigger time bins. A better analysis of the characteristics of the GRB can be done if the the frequencies of emission are to be plotted against the Fourier transform of the count rates. This enables viewing the light curve in the frequency domain. It shows which frequencies are present in the signal of trigger obtained and the amount of each of the frequencies that make up this signal. The Cooley-Tukey algorithm was the first algorithm ever used to work out this problem easily in the cases where the signals are very long. The so called Fast Fourier transform(FFT) is widely used in many present day analyses and researches.

The light curves of a GRB exhibits power-law behavior when its power spectrum is plotted. Power Density Spectrum(PDS) of a light curve is obtained by plotting the power of each signal frequency against the frequencies, where the power is calculated from the FFT itself. Further studying the power spectrum of the GRB gives us valuable information regarding its hardness, radiation mechanisms, whether it is a high or low energy emission and so on based on their power-law slope. A noise floor level is also plotted along with this power spectrum, so that the amount of noisy data can easily be recognized. The noise floor level is obtained from the measurement uncertainties values and implies the noise present in the data from the detectors due to uncertainties of measurement.

This report focuses on understanding the variability in the light curves of Gamma-Ray Bursts(GRBs) and quantifying this variability to interpret the differences between long and short GRBs. The objectives of this project include mainly plotting the light curves in time domain of a few GRB data obtained from the Fermi Gamma-ray Burst Monitor(GBM) and then finding their power-law slope and constant noise floor level. All these information gathered gives a better sense of various properties of GRBs and the variability among them, so as to differentiate between the two major classes of GRBs.

Chapter 2

Gamma ray bursts

Gamma-ray bursts are highly energetic explosions occurring in the universe emitting radiation in the gamma ray band of the electromagnetic spectrum. Radiations are so released in energies ranging from tens of kilo electron-volts to several mega electron-volts and for time period that can extend from several milliseconds to thousands of seconds. This duration of the bursts represents the temporal domain and the order of energies of these emissions, the gamma ray band represents the spectral domain of a GRB. This phase of the GRB is called as 'prompt emission', and it was discovered later that the emissions do not halt here. After this prompt emission phase there exists an 'afterglow' which lasts for much longer time frame and has varied wavelengths that constitutes this phase.

Figure 2.1: An illustration of Gamma-Ray Bursts as the most powerful explosions in the universe,Observation by NASA's Hubble Space Telescope (Credit: NASA).

The sources of such immensely energetic emissions is seen to be of two different types. One of them is associated with the termination of some massive stars, which results in supernovae. These kind of GRBs are the ones with a longer duration. The second type of origin of GRBs corresponds to compact star types which includes white dwarfs, black hole and neutron stars. The main mechanism involving creation of such bursts in this type is the coalescence of a system of one neutron stars and one black hole or a system of two neutron stars. GRBs of such classes have a shorter duration. In both classes of GRBs the emission is resulting from the cataclysmic events occurring in the corresponding systems that eventually leads to the formation of a rapidly-rotating magnetar or hyper-accreting stellar-sized black

hole. In the end central engines are obtained which causes the main part of a GRB which is the highly collimated relativistic jets, then further powered by both an expanding outflow and the continuous injection by the central engine(B. Zhang 2018).

2.1 Phases of a GRB

2.1.1 Prompt emission

The instrument used in detecting GRBs normally have a background emission spectrum. The duration is always taken in terms of T_{90}, which is the interval of time between 5% and 95% of the total counts that have been detected. Once the instrument starts getting a trigger of the GRB, the temporal phase of it that has emissions in the sub-MeV range excessively above the background levels of emission, is called the prompt emission phase of the GRB. X-rays that accompany the γ-rays as a low energy tail are the prominent bands of energy shown in the prompt emission(Piran 2005). The emission from the relativistic jet from an internal site where the ejecta consumes the energy through some internal processes like shocks or magnetic dissipation that are triggered internally, are the ones linked to prompt emission.

The two classes of GRB, which are different in their T_{90} spans, have their peak values around 20-30 second for long GRBs and around 0.2-0.3 seconds for short GRBs and their partition line is at 2 seconds from the observer frame of reference(B. Zhang 2018). These two classes can also be differentiated in terms of the hardness ratio(HR), the ratio of counts of photons in two different photon energy bands(higher and lower bands)(Ghirlanda, Bernardini, *et al.* 2015). It was observed that the short GRBs have a higher HR value than the long GRBs implying that the short GRBs are on an average harder than long GRBs.

The light curves observed for the prompt emission phase are highly erratic. This shows that most GRBs shows greater variability in the count rates when the time period chosen is less than the total extent of the burst. The elementary unit of such light curves are the individual pulses that makes up the overall plot for the burst. The peak energy of the light curve decreases exponentially with the photons counts detected and a hard to soft progression is seen. Analysing the temporal and spectral characteristics of these light curves shows that each pulses in it has a FRED(Fast Rise Exponential Decay) pattern. Moreover, depending upon the luminosities of the bursts, emissions of low energy ranges are delayed in comparison to those of high energy ranges. To put in other words, there is a lag-luminosity relation showing that long spectral delays are a feature of highly luminous prompt emissions. These spectral lags can be used to estimate the luminosities of the emissions to get more insight from their light curves. Wider light curves implies that the pulse are of low energies. There also exists a hardness-intensity correlation which depicts that spectral hardness is related to the intensity of the burst at a particular point in time. As the span of short GRBs is nearer to the limiting resolution of the detectors, varability of these GRBs is far more difficult to inspect than those of long GRBs(Piran 2005).

A portion of the GRB before the detection of the main burst, having comparatively lower peak magnitude than the rest of the emission is called a precursor emission. It is well partitioned from the actual burst by a background time period which is as long as the total stretch of the remaining emission. The properties of the main burst remain unchanged

regardless the presence of the precursor emission and the characteristics of these are also similar in most of the GRBs. Soft X-ray flares are also seen to tail the main burst and all these three components, precursor emission, main burst and X-ray flare can be connected with GRB central engine having irregular actions.

The features of a light curve can be studied in a more efficient way if the Power Spectral Density(PSD), which is the power defined as a function of frequencies in a GRB, can be plotted. This is achieved by obtaining the Fourier transform of the GRB light curve. If the time interval of an emission was periodic then the PSD would show sharp peaks at particular frequencies. But the PSD plot of a GRB shows no periodicity suggesting that the GRB central engines have no periodic behavior. On one hand, the PSDs of separate GRBs reveal noisy behavior and on the other hand taking average of PSDs of some GRBs detected by BATSE instrument onboard the Compton Gamma-Ray Observatory(CGRO) gave a power-law with an index -5/3 and for those detected by Swift satellite the index was steeper between the values -1.7 to -2.0. Such a power-law behavior implies a self-similar behavior for varying time scales suggesting random recognition of same events on different time periods(B. Zhang 2018).

2.1.2 Afterglow

Afterglows are the temporal phase that follows after the prompt emission phase that consist of all broad-band radiations from the GRBs and the span of this phase is longer, varies between minutes to months. Unlike the prompt emission phase that is observed in hard X-ray region and its characteristic of short time variability, afterglows, on the other hand, has emission detected in a wide range of radiation bands and exhibits simple decaying power laws. The radii of the afterglow emission zone is larger, i.e., greater than 10^{15}cm. The origin of afterglows is observed to be from the processes activated by the interaction between jets and the circumburst medium. The processes associated with the motion of the relativistic jets are the sources of GRB emission and such movement of these jets into the outside environment stirs up two types of impacts or shocks which are the forward shock and the reverse shock. Forward shock runs into the external medium while reverse shocks run into the jets. One of the radiations emitted by the accelerated electrons in the relativistic jets is the synchrotron radiation and these seems to be originated from the jets and outer medium that is in shock and separated by a contact discontinuity. Particle acceleration produced at these relativistic shocks also acts as a key component in the generation of afterglow. The extent to which the prompt emission phase dissipates the blast-wave energy and emits part of initial burst energy effectively determines the luminosity of the afterglow. Then the type of the progenitor is then the one that is completely related to the light curves and the spectra observed in the background during the outburst of GRBs(Miceli & Nava 2022).

The first part of the afterglow that commences even while the burst is occurring is the X-ray afterglow. It lasts for a short period of time and is the strongest among all other parts of the afterglow. The presence of afterglow is seen as the light curves produced several hours after the actual burst and it can be extrapolated to get the last stages of the prompt emission phase. The GRBs with optical counterparts for their afterglows are 5 times more brighter that those GRBs with no afterglow observed in the optical range(dark GRBs). Optical and Infrared afterglows are exhibited by almost 50% of the well bounded GRBs and

the magnitude is about 19-20 one day after the burst has happened. The optical spectra so observed decays as a power law, $v^{-\beta}$ and absorption lines can be superimposed on this power law. These absorption lines are the effect of the travel of the emission from source to earth.Without accurate localization of the GRB, the delay between the burst and the optical afterglow due to technical problems cannot be obtained. The cases where the optical brief flashes are not detected due to delayed and trivial observations or due to swiftly decaying or dim optical counterparts are then called dark GRBs(also called in the names Failed Optical Afterglows FOAs, Gamma ray bursts Hiding an Optical Source Transients GHOST). These have weaker optical complements minimum 2 magnitudes in R band than the GRBs having optical transients(OT). Almost 50% of the GRBs consist of a radio afterglow. As finding the afterglow falls abruptly at the two extremes(higher and lower frequencies), observations are mostly done in 8 GHz. The observed flux has a spike at about $2*10^{-29}$ kg/s^2 (2 milliJansky). Almost all radio afterglows are observed in X-ray, since the localization are based on X-ray afterglows. Nearly 80% of radio afterglows GRBs also have optical afterglows and similarly 80% of optically observed ones have a component in the radio afterglow region. the rest of the radio afterglows are dark in the optic region(Piran 2005).

2.2 Classifications of GRBs

2.2.1 Short Gamma Ray Bursts

Short GRBs are the ones whose T_90 duration is less than 2 seconds and have a hard spectral curve, meaning that its energies extend upto the ranges of mega electron volts(Ursi *et al.* 2022). Coalescence of compact binary stars is considered to be the origin of short GRBs. On an average, short GRBs have lower emittance and their fluxes have peaks similar to that of long GRBs. By calculating the hardness ratio of different GRBs it was seen that short GRBs have a harder energy spectra because of the harder low energy component(Ghirlanda, Nava, *et al.* 2009). These tend to occur at low redshifts and have substantially faint afterglows. The type of host galaxies that short GRBs are found in are late and early type galaxies which have low star formation rate. They also are corresponding to old stellar populations. Short GRBs are inconsistent with the E_{peak}-E_{iso} correlation, i.e., between the rest frame spectral peak energy and isotropic equivalent energy but are rational with the E_{peak}-L_{iso} correlation, where L_{iso} is the prompt emission isotropic peak luminosity. The evolution of massive stars in a primordial binary or dynamic interactions and seizure in globular clusters are found to be the progenitors of short GRBs. The merging of binary systems are required for the existence of short GRBs and such merging processes occur most of the time at the periphery or exterior to the galaxies also short GRBs exist in low density environments. Extended γ-ray emission which is softer than the initial burst of prompt phase occurs in almost 15% portion of short GRBs. Longer prompt phase time span and higher initial X-ray afterglow fluxes are the features of extended emissions and trademark of observed short GRB radiation powered by newly born magnetars are such soft extended emissions. Short GRBs have null spectral lags and larger projected physical offsets(D'Avanzo 2015).

2.2.2 Long Gamma Ray Bursts

Long GRBs are those whose T_{90} duration is greater than 2 seconds with softer spectrum and are related to the type Ic core collapse supernovae. The core collapse of massive stars is indicated as the progenitor for long GRBs. These are more energetic and have higher redshifts than short GRBs and their afterglows are also brighter. Long GRBs are consistent with both the correlations E_{peak}-E_{iso} and E_{peak}-L_{iso}. In a fraction of long GRBs, about 15% , a γ ray emission is observed as a precursor before the main burst and are associated with quiescent time which can be correlated to the T_{90} duration. Considering both the low-energy spectral index and peak energy, it can be inferred that the spectra of short GRBs are similar to the spectra of initial 1-2 seconds of the long GRBs. For only those bursts with high peak luminosities and those occurring at different areas in the lag-luminosity plot with reference to zero lag, low peak luminosity short GRBs, it is possible for the long GRBs to have a null lag. In the standard afterglow model divergence are found in long GRBs as a signature of it. Long GRBs are found to occur in star-forming galaxies and young massive stars are supposed to be the progenitors for these. Before the collapse with stellar wind, these massive progenitors fills the surrounding environment with metals. Long GRBs are linked to galaxies having rapid star formation rate and explicitly related to the death of these massive stars(Ghirlanda, Nava, *et al.* 2009; D'Avanzo 2015).

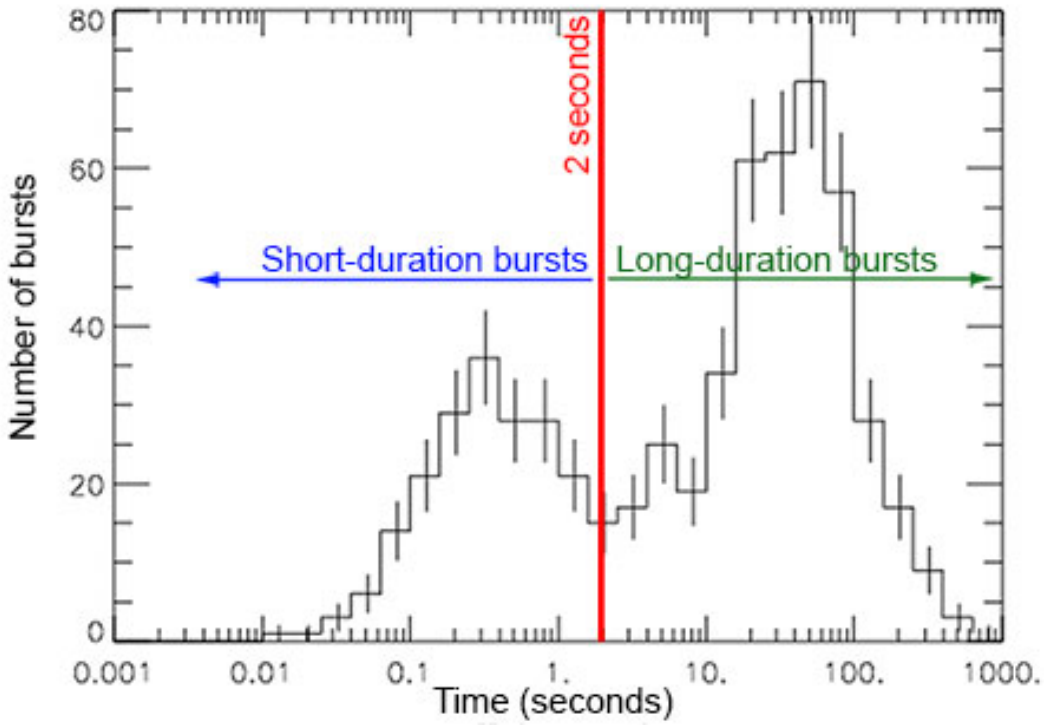

Figure 2.2: Plot of time versus number of bursts for GRBs observed by BATSE instrument on the Compton Gamma-ray Telescope (Credit:NASA).

2.3 Physical and radiative processes

When relativistic electrons undergo acceleration which is in a direction perpendicular to its velocity, then electromagnetic radiations are emitted which are called as synchrotron radiation. Among different radiation mechanisms, for a GRB synchrotron radiations of electrons accelerated in relativistic shocks were taken as the dominant mechanisms due to the fact that they have sufficient amount of energetic electrons and have strong magnetic fields in the region of emission(Y. Zhang *et al.* 2019). It was considered that synchrotron radiations were the sources of GRBs and later proved that from a power-law distribution of relativistic electrons with acute minimum-energy cutoff and an isotropic pitch angle distribution, an optically thin sychrotron spectrum is formed which becomes a good fit to some GRBs. Although, this simple synchrotron model could not explain some of the properties evident in the low energy range of GRB spectra(Lloyd & Petrosian 2000). Such a mechanism in the fast-cooling system interprets a low energy spectrum as $F_v \propto v^{-1/2}$, which is conflicting with the observations in most GRBs that $F_v \propto v^0$(Y. Zhang *et al.* 2019). It was also asserted that the spectral evolution of the low energy photon index, α, is inconsistent with the standard synchrotron concept, atleast when it comes to single shock model, throughout the burst. Therefore, the anomalous behavior of the spectrum of GRB needed explanations from some other models similar to Compton scattering to fixate the theory(Lloyd & Petrosian 2000).

A harder spectrum could be produced by an anisotropic pitch angle distribution which proposed that electron can be cooled down by Inverse Compton Scattering(ICS). Inverse Compton scattering is the process in which the energy gets transferred from relativistic electrons to photons, when the energy of the electron is significant enough as compared to that of the energy of photons and then the photons get scattered with a higher frequency. Since electrons implanted at an earlier time cool down slower than that in the constant magnetic field state, there will be a spatial decrease of magnetic field strength in the jet, which harden the prompt emission spectra. Adiabatic, synchrotron and ICS cooling mechanisms were included, after recent calculations, in the spatially decaying magnetic fields coherently. Harder low-energy spectra can be produced by both adiabatic/ICS cooling processes and deteriorating magnetic fields(Y. Zhang *et al.* 2019).

After considering leptonic processes whose origins are radiations like synchrotron and ICS, hadronic processes in proton-dominated GRB jets, are to be studied. In such jets, the acceleration of protons goes up as high as 10^{20} eV starting an electromagnetic cascade using the photomeson process in the photon field of the jet(Wang *et al.* 2018). The production of pions when photons collide with protons is called photo-pion process and the production of π^- is accompanied by production of atleast one π^+ for conservation of charge. Positrons which are capable of generating high energy photons through the synchrotron process are formed when a π^+ decays and a π^0 can directly decompose to two photons. In the situations where electrons are not able to be accelerated expertly to very high energies as protons are, the photo-pion process comes in handy. It also beat the maximum synchroton energy limit(Kumar & B. Zhang 2015). The intensity of the secondary $e^{\pm}$ pairs generated in the cascade can substantially exceed that of primary electrons in high energy range. The observed high energy spectrum can be regenerated from the synchrotron radiation and IC scattering of such pairs off keV/MeV photons in the jet(Wang *et al.* 2018).

The knowledge about the radiation process and on the geometry of radiating regions can

be obtained from polarization. The Stokes parameters of radiation emitted by each electron over the electron's distribution is integrated at first to get the observed polarization, which is called the local polarization. Then integration is done over the emitting region to yield the global polarization. The radiating region moves relativistically to the observed region in both the phases, prompt emission and afterglow, of a GRB. The Lorentz transformations thus indicated has a significant role in the second integration because in that case the direction of propagation of photons and hence the direction of local polarization changes. The polarization in the same direction is reduced to 70% after integration over the emitting region even if initially the intrinsic emission is 100% polarised in the same direction. For example, in the context of synchrotron emission, it is polarised with intrinsic local polarization level depending upon the emitting electron's spectral index of energy distribution. For typical values of this spectral index, the level of local polarisation can go upto 75%. The magnetic field and the direction of emitted radiation lies perpendicular to the polarization vector. The Inverse Compton Scattering for which the intrinsic local polarization is higher, going upto 100% when the photons are scattered at 90^o, can also be formulated using this concept(Piran 2005).

2.4 Progenitors

An astrophysical system that precedes the GRB and causes the burst through a catastrophic self-destruction are known as progenitors. Analysis of afterglows and host galaxy of GRBs led to the classification of their progenitors into two major categories. Supernova type Ic are observed to be the progenitor for most of the long GRBs whose host galaxies are recognized to be dwarf star-forming galaxies. Short GRBs, on the other hand, have early or elliptical-type galaxies with little star-formation as their host galaxies and some others are present in star-forming galaxies also. Hence, all these observations led to the realization of another type of progenitor which rather than being related to massive stars are related to compact stars like NS-NS or NS-BH mergers. About a week after the main trigger for a long GRB, a supernova red bump in the optical light curves can be observed. Large offsets are detected for many short GRBs from their host galaxies and some of them are also hostless since they cannot be found near the GRB afterglow region. Also, for some short GRBs the host galaxies are detected in the far vicinity of the GRB indicating that the GRB might have been kicked out of that galaxy(Kumar & B. Zhang 2015; B. Zhang 2018).

2.5 Some other properties

Considering some other temporal properties of GRBs, it was proved that the light curves of GRBs are the superimposition of a slower and a faster component. It was seen that at low energies there is a gradual reduction in the fast component but in a step wise low-pass filter correlation analysis it is evident that there is a distinct low frequency component. Pulses of light curves are narrower in harder bands, i.e., light curves are varying with energy bands. The width ω of the pulses is a function of energy E as $\omega(E) \propto E^{-\alpha}$. Spectral properties include that GRB light curves are non-thermal and are time integrated spectra. As some

GRBs exhibit strong spectral evolution, time resolution of the information is really necessary in the analysis of the light curves. This can be done for only bright GRBs as the time bins chosen for plotting the light curves cannot be infinitesimally small but have enough photon counts within them to get a reasonable spectral fitting. [17] A typical GRB spectrum can be fitted with a smoothly joined broken power-law known as the Band function if the detector's energy band is wide enough. When obtaining the prompt emission spectrum of a GRB it can be seen that there are three components to it which are a non-thermal Band component, a quasi thermal component and another non-thermal component that can be fit as a power-law approaching higher energies(Kumar & B. Zhang 2015).

Chapter 3

Instrumentation and Techniques

3.1 Fermi Gamma-Ray Space Telescope

The Fermi Gamma-Ray Space Telescope was launched into a 565km orbit with an inclination of 25.6 degrees and have a payload consisting of both LAT and GBM. The Gamma-ray Burst Monitor(GBM) was developed originally for the joint investigation of spectra and time information observed of GRBs by both GBM and Fermi Large Area Telescope(LAT). The role of LAT is to make observations in the high energy range, above 20 MeV from different astrophysical sources. GBM, on the other hand make measurements in the low energy range, at nearly 8keV to 40MeV, so as to enhance the knowledge available from the Fermi about GRBs. The spectra of bursts in over seven decades in energy are thus gained from the LAT-GBM combination(Meegan *et al.* 2009).

3.1.1 Large Area Telescope(LAT)

The Large Area Telescope(LAT) aboard the Fermi Gamma-ray Space Telescope is a pair-production telescope which uses silicon strip trackers, a Cesium Iodide calorimetre and a plastic scintillator anti-coincidence system. It has a field of view of 2.4 steradians and covers energy range between 20 MeV and above 500 GeV. Using the figures of electron-positron pairs, produced when the γ-rays encountered by the LAT interacts by pair-production in the field of an atomic nucleus, arrival time, arrival direction and energy for individual photons can be derived. There are three subsystems of detectors for the LAT. These are:

- The Tracker, which convert the γ-rays and gives the arrival direction information. These are 18 x-y pairs of single-sided silicon strip detectors and tungsten converter foils are used to interleave the first 16. There are a total number of approximately 880,000 data channels in them and in the primary trigger mode a signal is produced when the tracker system self-triggers on a pattern of three consecutive x-y pairs.

- The calorimetre, carries out the measurement of energy and comprise of 1536 cesium iodide logs which are stacked in 8 layers and read out by custom photodiodes. The form of high-energy showers can be measured because of its hodoscopic structure.

Figure 3.1: The Fermi Gamma-Ray Space Telescope being prepared for launch vehicle integration at Cape Canaveral. On top is the LAT with its reflective covering. Six of the GBM NaI detectors and one BGO detector can be seen on the side of the spacecraft. Photo credit: NASA/Kim Shiflett(Meegan *et al.* 2009).

- A system of 89 single plastic scintillator tiles overlapped, with scintillating fibres covering seams is the LAT anti-coincidence system. The photomultiplier tubes measure signals from charged particles.

Extensive Monte Carlo simulations are used to enhance the performance and design of the LAT and the same type of simulation package is equipped in developing automated analysis steps for the data. This type of analysis done on the data stream differentiates pair production events from unwanted triggers and calculates the energy and arrival direction of each event. Re-analysing data to get advanced information of the telescope and also its space environment is possible now for the LAT team because of this automated system. Many advancements happened in the performance of satellite since the time it was assembled, like improved angular resolution and the new analysis method developed from the flight experience elevated the rate of γ-rays detected by about 30%. The LAT has been operating for more than 13 years now and it has not undergone any serious hardware failures, instead have been functioning more better than before as a result of several upgrades done on

it(Thompson & Wilson-Hodge 2022).

3.1.2 Gamma-ray Burst Monitor(GBM)

While the primary aim of setting up GBM is for joint analysis with LAT, other objectives include obtaining near-real time burst locations on-board so that the spacecraft re-pointing is possible and LAT can make measurements of the delayed radiations from the bursts. The locations so obtained are also immediately circulated to all the ground-based observing instruments. GBM has an on-board software that identifies and localizes the burst over entire unocculted sky then transmits the data to LAT and ground observatories. Data obtained from the GBM system adds upto a catalog containing spectral, temporal and localization information of a GRB. If for any GRB, like strong GRBs detected by GBM, additional observation data are needed for extended time period(nominally five hours), then the spacecraft is re-adjusted so that they can be further analysed by LAT. GBM is not only useful in observing GRB triggers but can also be used to transmit data that are needed for a number of other investigations. The background data that are continuously transmitted to the ground contains information about triggers of solar flares, Terrestrial Gamma Flashes(TGFs) and Soft Gamma Repeaters(SGRs).

The scintillation crystals present in the GBM detectors enables the identification of hard X-rays and γ rays as they interact with these crystals. The light produced in the scintillation crystals when a γ ray falls on them, is detected by the photomultiplier tube attached to the detectors. This in turn gives an idea of the energy of γ rays as the number of photons produced in the crystals are proportional to this energy. The hardware system of GBM consist of twelve Thallium activated Sodium Iodide(NaI(Tl))scintillation detectors, two Bismuth Germanate(BGO) scintillation detectors, a Data Processing Unit(DPU) and a power box. The twelve NaI(Tl) detectors are arranged in groups of three on each corner of the spacecraft and the two BGO detectors are oriented on each side of the spacecraft. This ensure the detection of GRBs from any part of the unocculted sky. The crystals in the NaI(Tl) detectors are of cylindrical shape having the dimensions of 12.7 cm diameter and 1.27 cm thickness and is coupled with a photomultiplier tube(PMT) of 12.7 cm diameter in size. The energy range required to be detected for GBM i.e., 8keV to 1MeV, is enabled by a Berillium entrance window which makes these detectors sensitive in that range only. Each BGO crystals consist of a cylindrical shaped crystal which have 12.7 cm diameter and length. Each end of the BGO detector is coupled with a PMT rather than a single PMT, hence provided better light collection capacity to the detector. The BGO detectors have detections in the energy range 200keV to about 400MeV and thus acts as the bridge between the energy ranges of NaI detectors and the Fermi LAT. There are four energy bands covered by NaI detectors which are 8-50 keV, 50-100 keV, 100-150 keV and 150-300 keV bands. In addition to this, two energy bands for the two BGO detectors which are 0.3-1 MeV and 1-10 MeV and two others are covered by the LAT Low Energy(LLE) technique which are the energy bands 10-100 MeV and 100-1000 MeV(Bissaldi *et al.* 2015).

The digital processing unit(DPU) develops the signals from the detectors and are digitized into 4096 linear energy channels. If the signals so produced exceeds a particular programmable threshold, the peak height of the pulse is measured and transformed into 128 energy channels, which constitute the CSPEC continuous data type and 8 energy channels

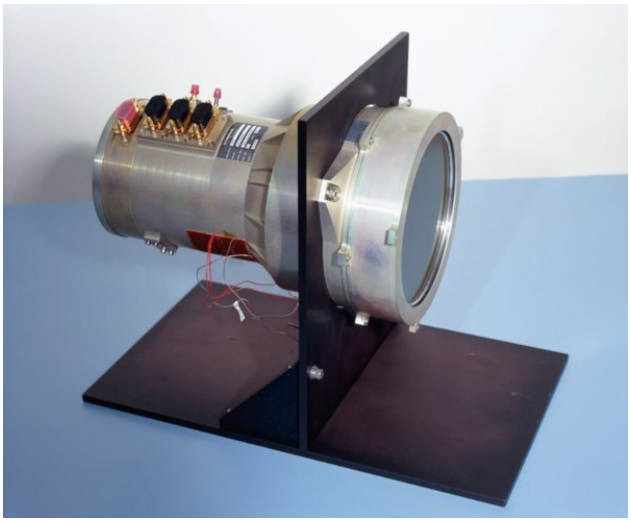

Figure 3.2: Fermi GBM NaI detector(Meegan *et al.* 2009).

Figure 3.3: Fermi GBM BGO detector(Meegan *et al.* 2009).

of CTIME continuous data type. Programmable look up tables are developed for providing boundaries for the channels of each data type. The channel widths must be compatible with the detector energy resolution which is defined as a function of energy and look up table are set taking that into consideration. Programmable resolution for counts accumulated into the time bins are done for CSPEC and CTIME data types and have default values of 4.096 s and 256 ms respectively. Time-tagged event(TTE) data provides individual counts along with 128 channels in match with the CSPEC data, detector identification and a time resolution of 2 μs. Originally, TTE data were only provided for 330s, 30s before burst trigger to 300s after the burst trigger. In 2012, continuous TTE(CTTE), was made by a GBM flight software update,v which now is available every time the instrument is working. At the GBM Instrument Operation Centre(GIOC) the predominant data from the GRB are gathered into two data types, continuous data and trigger data, as Flexible Image Transport System(FITS) files. For each one of the GBM's 14 detectors, CSPEC and CTIME data are

stored into daily files which comes along with daily spacecraft position history files and are delivered to the Fermi Science Support Centre(FSSC) whereas CTTE data are packed into hourly files as they are quite large. DPU has the functions of developing signals from the detectors, regulates high and low voltage to the detectors, processes commands and formats data for transmission to the spacecraft. A single printed circuit board is where all the DPU functions are implemented and there are two such boards. Some functions like pulse height analysis(PHA) and transmission of time-tagged events(TTE) data are carried by the hardware, while some other functions like GRB triggers, GRB localization and Automatic Gain Control are carried out by the flight software.

When in two or more NaI detectors, there is a spike in the count rates above the background rates and go beyond the programmable threshold value, then there forms a trigger in the Fermi GBM. Time spans of triggers are pronounced in multiples of 16 ms upto 8.192s and no timescales longer than 4.096s are in use presently. The energy range used by the algorithm used for triggering is in between 50-300keV and the ranges 25-50keV, >100keV and >300keV are also in use for some algorithms. Algorithms that use BGO detectors upgraded for finding terrestrial γ-ray flashes accompanying lightning. Alert data are telemetered to the ground instantly via the Tracking and Data Relay Satellite System(TDRSS) whenever a trigger occurs. The information contained in these data packs are the trigger time, trigger significance, the on-board localization, the trigger classification, hardness ratios, detector rates that caused the trigger, background calculated on-board and a light curve. In the case of GRBs, these alert data packs are also transferred to the FSSC along with the important spacecraft position data and altitude data as TRIGDAT FITS files.

A variety of data on burst triggers are transmitted from the GBM to the LAT. This gives the capability to reconsider event filters to enhance the GRB sensitivity, refine the location or update a GBM repoint recommendation. An immediate trigger signal within 5 ms, generated by every GRB and a set of five calculated data packets which begin 2s after the trigger are sent to the LAT. The five sets include event localization and categorization, the trigger time and timescale and energy range in which the trigger was produced. Together with all this, a single repoint request message is also sent specifying whether or not these satisfy the criterion for repointing the spacecraft. LAT also transfers data to the GBM during triggers to which the GBM react by reducing the real-time telemetry rate so as to not cause conflicts with the LAT real-time data. Along with the localization of source of the GRBs with GBM, it uses the relative rates of the direction of the burst in each one of the 12 NaI detectors to calculate the most probable arrival direction. Angular and spectral response of the detector is taken into account in the algorithm for pinpointing the position. The flight software on-board the GBM figures out the relative burst rates in each detector by using the average background rates excluding initial 4s after the burst and only choosing those during the last 17s of the trigger. An enhanced automated localization, called RoboBA, is calculated using the full trigger data set, on the ground.

Fermi GBM, with the help of its wide field of view can observe a large variety of astrophysical phenomena over the entire unocculted sky. These include accreting pulsars, magnetar bursts, X-ray binaries, GRBs, solar flares and TGFs from lightning. 3151 GRBs, 418 magnetar bursts, 1202 solar flare and 1160 TGFs have been triggered on the Fermi GBM, as of September,2021. GBM Accreting Pulsar Program(GAPP) specifically detects X-ray binaries and Accreting pulsars which are only triggered on GBM rarely(Thompson & Wilson-Hodge

2022).

The primary data products that is sent to the ground for analysing is the raw data which are provided by the spacecraft telemetry and are studied further by the Fermi Mission Operations Center(MOC). No information is lost but same data are removed, quality-checks are done and data packets are ordered according to time, in the case of level 0 data which undergoes minimal processing. Raw telemetry is the one transformed into level 0 data at the MOC. The starting point for scientific study by the users and the GBM instrument team is served by level 1 data produced by the automated pipeline processing of level 0 data. Continuous data are the rates in all GBM detectors in every energy band even if the burst has not occurred. Level 1 data consist of this continuous burst data which are rates, counts, catalog information and additional data required for analysis of GRBs. Daily, burst and updates are the three categories of data products sent to Fermi Science Support Center. Daily data products includes all the data taken continuously regardless of whether the burst has taken place or not. Hence, these contain all the rates from all the detectors, detector calibrations monitored and spacecraft orientation and current position. The files related to a given trigger that are obtained and sent to FSSC within a day after the burst are called burst data products. Count lists, binned counts and Detector Response Matrices(DRMs) and necessary background spectra constitutes burst data products. The last category of GIOC data products is the updated data products sent to FSSC periodically that includes corrections that do not change with time or changes slowly. Trigger, spectral and burst catalog are in this category. A primary version of the burst catalog file is sent along with other burst data and a number of updates files are sent eventually by the time the burst data has been re-checked again(Meegan *et al.* 2009).

3.2 Methodology

3.2.1 Obtaining the light curve

The data obtained from the detectors of Gamma-ray Burst monitor are used to develop a plot of photon count rates from the detected γ-rays versus the time values, which is called as the light curve plot in the time domain. For extracting the data, the GBM detectors that are triggered by the burst are selected but if there are more than three of the triggered detectors, not all of them are used for the purpose. Only those three detectors which were pointing closest to the emission location are taken into consideration. To take global fluctuations, an initial study on the raw time data is accomplished which characterizes the background. To identify all radiation periods from the triggered GRBs in which the γ-ray activity is ascertained, background subtracted light curves must be obtained. Initially, a steady background fit is measured between 1000s and 800s before t_u, which is the GBM detector trigger time. This is done for more than 90% of the bursts and marks the start of the observing time interval. 50s after the end of the Fermi T_{90} interval, which is the central time window which consist of 90% of the fluence of the GRB, is taken as the end time of analysis interval.

The selection of background time periods in which no gamma-ray emissions are detected are now automated. An algorithm identical to the Fermi-GBM online trigger that correlates the observed rate to a prediction based on a fit to the rate at previous times, is used for the

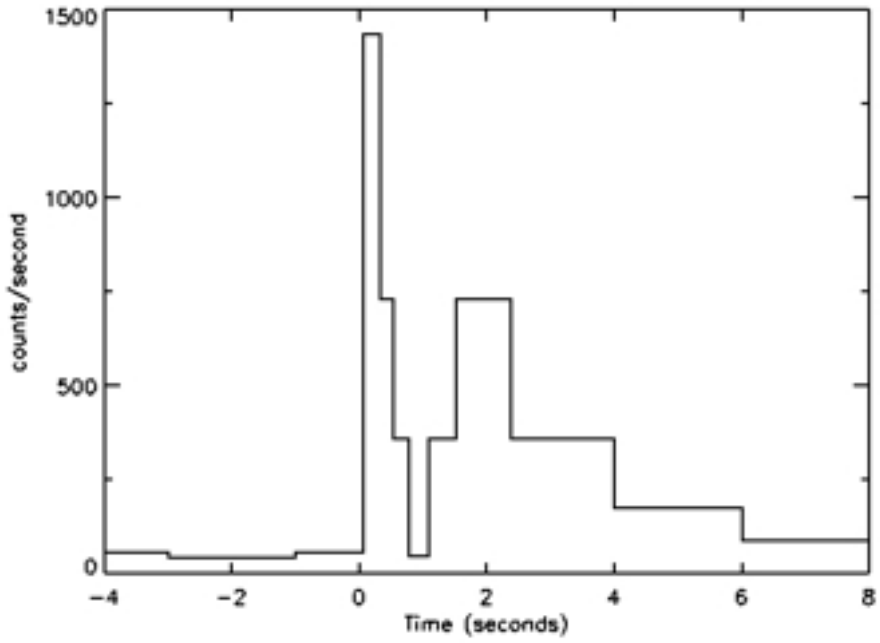

Figure 3.4: The light curve plot of the first GRB detected using Vela IVa satellite(Kouveliotou *et al.* 2012).

determination of background intervals with a requirement that the rate does not undergo a sudden hike. Then the extrapolation to the intermediate regions of the rate in the recognized background intervals gives us a fully data driven evaluation for the background rate over the total light curve(Coppin *et al.* 2020).

The background counts are then subtracted from the observed counts to get the net counts which are then used to calculate the count rates. The count rates are obtained by dividing the net counts by exposure time and are plotted against the centroid time values, which are clipped to get the time period during which the burst triggered the detector, to get the light curve in time domain. This light curve is used in our further analysis. It shows the time bins when the burst triggers the detectors of GBM and the rest of the time bins when no trigger occurs, thus plotting the background rates.

This light curve is further used in the analysis to find the Fourier Transform(FT) for obtaining the light curve in the frequency domain. Such a frequency domain is plotted with the frequencies present in the signal from the detector against the Fourier Transform values which can be calculated using Fast Fourier Transform.

3.2.2 Fast Fourier Transform(FFT)

The observations in an astronomical problem is assumed to be inhibited within an infinitely-long, smooth signal which can either be the plot of intensity variations with wavelength in a spectrum or any other measurable quantity like wavelength or position, that varies with time. Because of constructive difficulties when it comes to the inversion of convolution

integral in the presence of noise, the frequent problem of amendment of astronomical data sets for smearing effects(restoration), was not solved. The noisy portion in the basic signal that can be covered by the analysis, is only finite and are caused by the variations either inherent in the signal or that produced by the apparatus(Brault & White 1971).

Fourier analysis is done on a light curve to obtain the frequencies of component sine and cosine curves that make up the required light curve. Every curve of different frequencies and wavelengths can be broken down to a number of sines and cosines of different frequencies because the superposition of these component curves will give us the required curve(Brault & White 1971). The well-known equation of of Fourier transform is given by

$$F(\omega) = \int_{-\infty}^{\infty} f(t)e^{-i\omega t}\,dt \tag{3.1}$$

The Fourier analysis of such light curves with their data discrete, instead of continuous data, requires a Discrete Fourier Transform(DFT) to get the Fourier Transform of the curve. In DFT, the component sine and cosine curves are found by multiplying the data points with those frequency valued sine and cosine signals whose time period corresponds to the one period of the required signal, to get their correlation and thus the amplitude in which those frequencies are present. The highest frequency possible is the one whose period is equal to the duration of the signal and other frequencies will be the integer multiples of this frequency. The number of frequency bins will thus be equal to the number of data points in the signal. Therefore, DFT involves multiplying N data points with N different frequency signals, that is O(N^2) calculations. If f_j denotes the value of f(t) at t=t_j, then DFT is defined as

$$F_p = \sum_{j=0}^{N-1} f_j e^{2\pi ijp/N}\ ; p = 0, 1, 2, ..., N-1 \tag{3.2}$$

where f(t) is defined at t_i = 0,1,2,..., N-1(Sastry 2012). The signals from the GBM detectors which are of very long time periods will then involve large number of DFT calculations. Since this is a cumbersome process, J. W. Cooley and John Tukey together came up with an algorithm that reduces the order of multiplications from O(N^2) to O(Nlog(N)).

The practical application of Fourier analysis as a solution to the problems of smearing effects on the data, is now privileged as the FFT algorithm reduces the computing times to very tolerable values. To have a Fourier representation of discrete data of a signal will be suitable for use in both spectral analysis problems and restoration when the conditions provided by the sampling theorem are satisfied. An idea of how much variation corresponds to a given time scale is obtained from the absolute value of coefficient associated with the cosine term, from the exponential part of the Fourier transform calculated. The Nyquist frequency is the highest frequency of variation which gives the limit for the number of frequencies at which the data can vary for a discrete time series(Brault & White 1971).

The method by which Cooley-Tukey algorithm reduces the order of calculations in finding the Fourier transform was developed when computing the frequency waves that correlates with the period of each data point, the overlapping of different frequency sinusoidal waves at each data point was observed. Therefore, the repetition can be reduced for each data point when we consider the frequencies which have the same value for that point and calculate the sine and cosine values only for the frequencies that do not overlap. The calculations

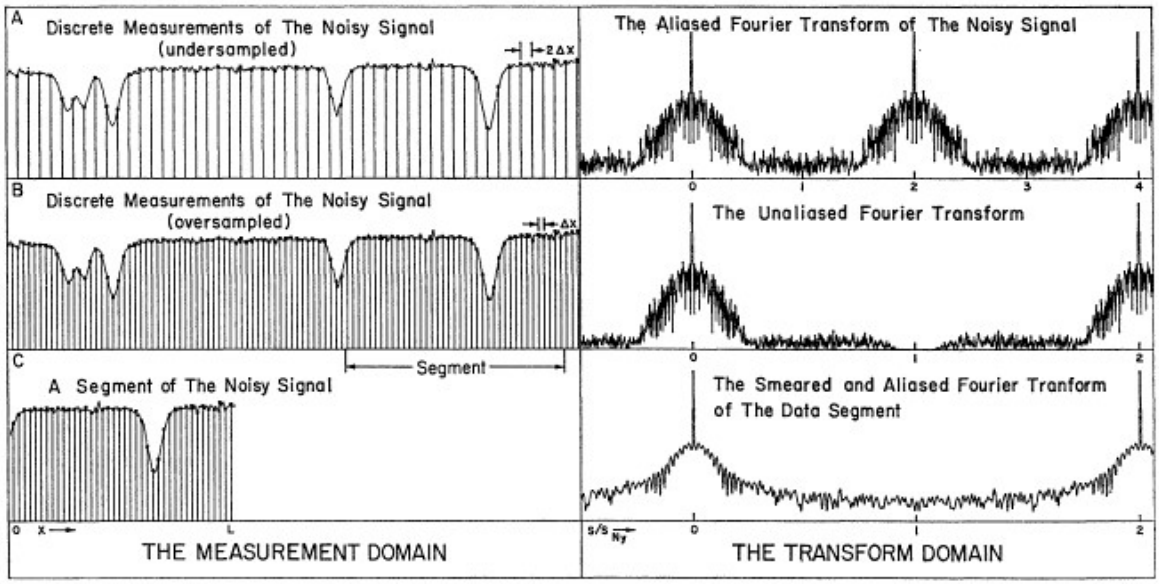

Figure 3.5: Plots showing the effects of sampling and finite measurement length in both measurement and transform domains(Brault & White 1971).

that are repeated are found by splitting the data sets into even and odd indices. Their multiplications with the frequencies shows that the first half of the data points have the same value for the sine waves as the second half in the even-numbered data points and the first half have negative value of the second half for the sine waves in the odd-numbered data points. The calculations are thus reduced by half because we need to evaluate only the value in either half for both cases. But for the calculations to be reduced to O(Nlog(N)), the splitting into even and odd data points is continued until one data point is reached by evaluating the similarity of the sine waves and thus limiting the calculations in half in every division.

The time(centroid time) values are centered by subtracting the first element of the data set from the sequence of values. Then the count rates obtained before are interpolated as a function of the independent variable, time, because the rates are to be specified for all time values, in case they are not calculated at a particular time of the sequence and this is made possible by linearly interpolating count rates with respect to time. Thus, a sequence of count rates(flux) are obtained which are then normalised by subtracting the mean value of these flux data from each value of the obtained sequence. Python Programming consist a module called Scientific Python(SciPy) which has a package called fftpack() which helps in finding both the frequencies and the FFT values of the signal using the attributes rfft() and rfftfreq() of this pack. rfft() attribute when operated on the normalised flux will give us the FFT values and rfftfreq() operated on the size of the FFT sequence or the number of data points under consideration, along with the time interval between two time points give us the frequency points corresponding to those FFT values. Plotting the evaluated frequency values against the FFT values gives us the light curve of the data set in the frequency domain. This plot shows the amount of distribution of various frequencies that constitute the GRB trigger

signal. This is further used in the spectral analysis to know more about the nature of the GRB.

3.2.3 Power Density Spectrum and noise flooring

Power Density Spectrum(PDS) of a GRB signal is its measure of power as a function of frequency obtained using the available data from the light curve in time and frequency domains. Even after comprehensive statistical studies, the temporal behavior of GRBs is still not understood completely as the light curves of these mostly have many irregular peaks. Significant information on GRBs are obtained when we analyse the PDS of long gamma-ray bursts because it implies a self-similar temporal structure. The longest GRBs for which the T_{90} duration is greater than 100s exhibit the best power-law PDSs in which more than 2 decades is covered by the range of self-similar time scales.

The statistical variations strongly influences the apparent PDS slopes of shorter bursts. By averaging the PDSs for a very large sample of GRBs the elemental power-law can be reproduced with a higher accuracy and the power-law slope so calculated has a value of $\alpha = -5/3$. The power-law PDS puts forward a new susceptible tool for the analysis of gamma-ray bursts. For hard energy channels($h\nu > 300keV$) the PDS flattens and for soft energy channels($h\nu < 50keV$), the PDS steepens, whereas for bolometric light curves the power spectrum obeys the -5/3 law approximately. As opposed to the complicated varied behavior of long GRB light curves in the time domain, they display a simple nature in the Fourier domain. In addition to the -5/3 power law index of their PDS, an exponentially distributed analytical fluctuations are also superimposed onto their power-law. The process is characterized randomly by the -5/3 index and a sharp break at 1 Hz, which generates the diverse light curves of the GRBs. Individual bursts display power-law behavior and cans be used as a clue to study the characteristics of the GRBs. Chiefly, the analysis of PDS slope can be done for separate energy channels and differences of the temporal behavior between the channels in reference to their power-law indices can be assessed(Beloborodov *et al.* 2000).

The Power Spectral Density or the PSD value for each data point is calculated by multiplying the respective FFT values with their complex conjugate, or in other words taking the square of the absolute value of the FFT, and then dividing it by the sequence size of flux values multiplied by the time interval between each time point, as a part of normalizing the PSD. Also the term $(2T/\mu^2 N^2)$ is again multiplied to this value to get the fractional rms-squared-normalised power spectrum values, where T is the total monitoring duration of the burst and N is the number of data points and μ is the mean of light curve(Goyal 2021). Thus, the power values are given by the equation

$$P = \frac{2T}{\mu^2 N^2}\left[\frac{|FFT|^2}{L \times dt}\right] \tag{3.3}$$

where L is the length of the flux array and dt is the time interval between two time data points. The power(P) calculated are converted into their logarithmic values and stored in an array which are then plotted against the logarithm of frequencies(F) obtained before. The loglog() attribute within the matplotlib module of Python enables us to get the logarithm of power array to be plotted against the logarithm of frequency array. This gives us the power

spectrum of the GRB and depicts the variations in the power that each frequency points possess.

The power law index(slope) can be obtained by fitting a power-law function corresponding to this spectrum. The power-law function that needs to fitted is given by

$$Power = C \times Frequency^{-\alpha} \tag{3.4}$$

where C is some constant and α gives the power-law index. When the parameters, power and frequencies, are plotted using this equation in the logarithmic scale then the equation becomes

$$\begin{aligned} log(P) &= -\alpha \times log(F) + log(C) \\ \Rightarrow log(P) &= -\alpha log(F) + \beta \end{aligned} \tag{3.5}$$

where $\beta = \log(\mathrm{C})$. As this equation is in the form of a straight line equation, we can also do the power-law fitting by finding the logarithmic power and frequency values of the sequence and fitting a straight line function using these logarithmic parameters, which gives us the same equation as above. The best fitted straight line is plotted against the logarithmic frequency values in the X-axis, in the same plot of the power spectrum. The parameters α and β of the best fitted curve is then obtained of which -α is the required power law index. The power law index are calculated and tabulated for the GRBs and they provide valuable information regarding the nature and hardness of the GRB signal.

The noise level in the PDS due to uncertainties in the measurements needs to be taken into consideration. The noise floor level is plotted in the same power spectrum and the power-law fit plot. This enables us to identify the power values that can be taken under consideration for our analysis and that way we can remove the noise present in the signal due to certain measurement uncertainties. The uncertainty values are obtained from the data set of each GBM detector which are triggered by the GRBs. This constant noise floor level is evaluated using the equation

$$P_{stat} = \frac{2T}{\mu^2 N}\sigma^2_{stat} \tag{3.6}$$

where σ^2 is the mean variance of the uncertainties ($\Delta f(t_i)$) on the flux values in the light curve at times t_i given by

$$\sigma^2 = \sum_{i=1}^{N} \Delta f(t_i)^2/N$$

So, within the same plot it will be possible to produce the power-law index by fitting the straight line function of logarithmic parameters and the noise floor level portraying the level upto which noise is produced in the PDS due to the uncertainties in the data obtained(Goyal 2021).

Chapter 4

Results and Discussion

The analysis of GRB data available from the Fermi GBM using Fast Fourier Transform(FFT) was done with the intention to infer the variability in their light curves and power spectrum and obtain the level upto which this variability can be studied. Gamma-ray Bursts, as mentioned in above sections, are highly energetic and most luminous explosions in the universe and there are only two major types of them, short and long GRBs. In this analysis, burst data including the photon counts, background counts, net counts, centroid time of burst and the measurement uncertainties, from the Gamma-ray Burst Monitor(GBM) is collected and their light curves and power spectra with power-law curve fit and noise floor level are plotted using Python Programming. The power-law index and noise floor level are obtained from the plots and they depict the different characteristics of GRBs which are deciphered and studied. The graphical representations for data collected from three detectors of the Fermi GBM of each GRB are given as results and the power-law indices and the constant noise floor levels are tabulated in this section.

4.1 Light curves

The burst data for 10 GRBs are collected from the detectors of Fermi GBM and light curves are plotted only for those detector's data which are pointing closest to the burst location. Also the binning time in which the data of burst are collected can be different too and here those data sets of detectors whose binning time is lowest is chosen to get a more refined picture of the burst characteristics. The 10 GRBs for which this analysis is done is listed below:

1. 080916C
2. 090510
3. 120323A
4. 130427A
5. 150101B
6. 170206A

7. 180720B
8. 190114C
9. 200826A
10. 220627A

The data file consist of centroid time when the burst was detected, exposure time, photon counts, background counts, net counts and the measurement uncertainties. The count rates are then calculated using the equation mentioned in the previous chapter and are plotted against centroid time for each data point to obtain the light curve in time series. These light curves gives us the information about which GRBs are short GRBs and which are long ones. This can be done by observing the time period of burst peak in the light curve, excluding the background count rates on either side of it, and thus checking their T_{90} duration. There are 5 GRBs which are observed to be long GRBs and 5 are short ones. The analysed short GRBs are

1. GRB090510,
2. GRB120323A,
3. GRB150101B,
4. GRB170206A and
5. GRB200826A.

The rest of the GRBs which belong to the class of long GRBs are

1. GRB080916C,
2. GRB130427A,
3. GRB180720B,
4. GRB190114C and
5. GRB220627A.

After taking the FFT of these count rates and with their array size we get the frequency components and the amount of each such frequency present in the burst signal. This is used to get frequency domain of the light curves.

4.2 Power Density Spectrum(PDS)

The power spectrum of each GRB light curves are obtained by substituting the FFT values obtained in the power equation(3.3). The plots of power versus frequency values are generated for 10 GRBs and power-law fitting(3.5) and the PSD index or slope values are calculated which gives an insight about the variability found in the GRB light curves. This is done for each detector data selected for a GRB and the difference between their variability are inferred from the index values. On an average the power-law index is seen to be about -1 for the BGO detectors for all 10 GRBs and it is around -1 to -2 for the NaI detectors. The frequencies used in getting the power values for plotting the PSDs of these 10 GRBs are temporal frequencies which implies that the variability observed is a correlated colored-noise type stochastic processes. It is stated that when the power law index of the GRB power spectrum α= 0, it conforms to uncorrelated, white-noise type stochastic process. Precisely, α= -1 is known as long memory/pink noise type stochastic process and α= -2 corresponds to damped-random walk/red-noise type stochastic process. The white noise is characteristic of GRBs that are dim because they have low signal to noise ratio and hence are overshadowed by Poisson statistics. The autocorrelations in the variability of GRBs persist throughout the light curves and therefore the random component enclosed in the γ-ray signal is structured on a fundamental level. Then the noise flooring is done on the same power spectrum and the level of constant noise floor is found for each plot which explains the point upto which the variability can be studied in the PDS and the rest is considered to be noise dominated(Tarnopolski & Marchenko 2021).

The plots for all 10 GRBs containing the light curves and power spectrum of each selected detector of that GRB are provided below.

The results have been tabulated in Table:4.1 containing the GRBs that are analyzed with the time period of data chosen to plot the light curves and the detectors' data chosen for each GRB. The power-law index values and the constant noise floor level are the measured results.

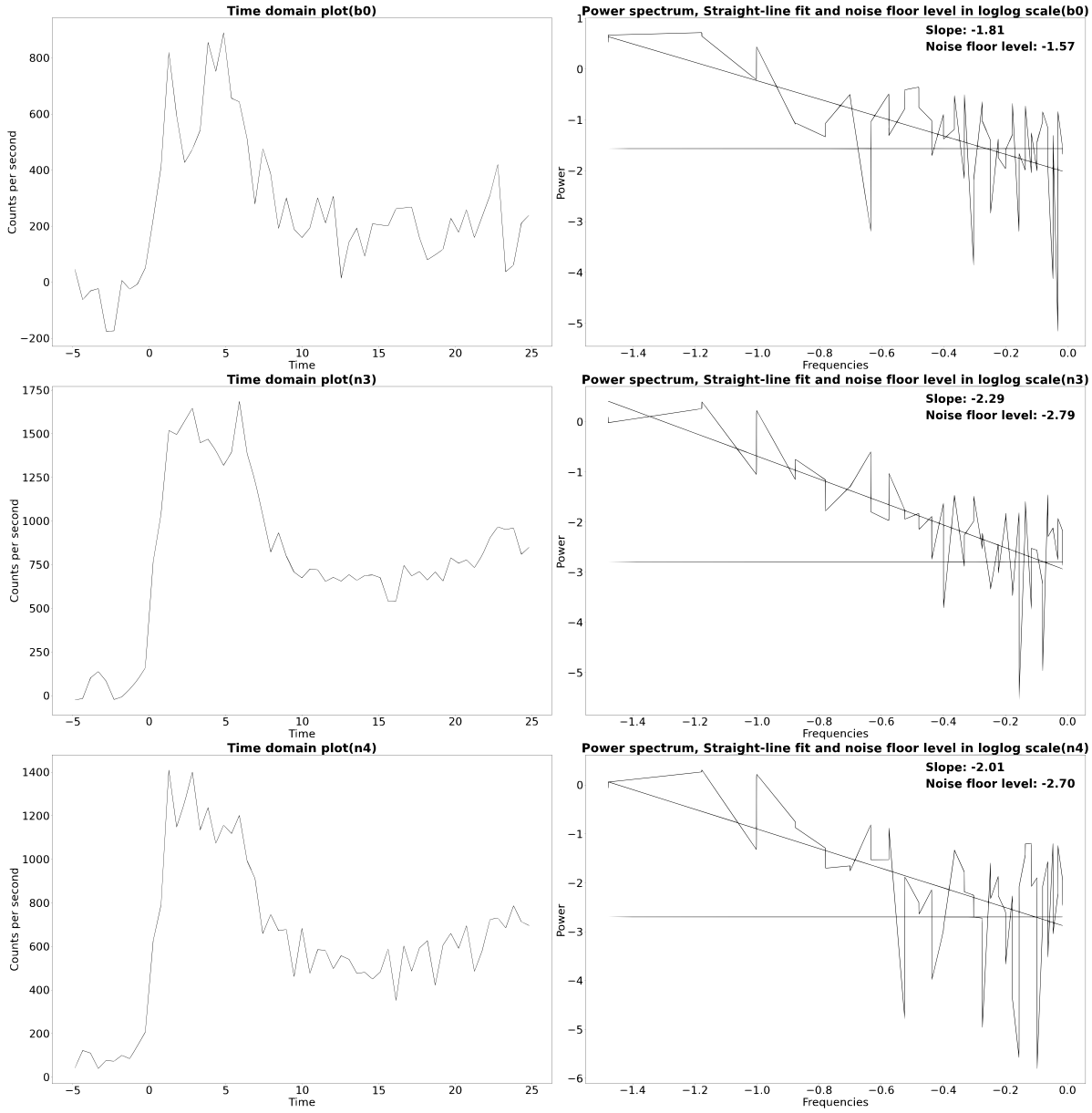

Figure 4.1: The multiple plot consisting of light curves and power spectra of data obtained from three detectors for the GRB080916C. The data from one BGO b0 detector and two NaI detectors n3 and n4 are used for the analysis of this GRB. The trigger time for all these detectors were from -5 to 130 seconds. The burst time was observed to be between -5 and 25 seconds and here LC and PSD are obtained for that time. Based on this burst time it is evident that the GRB080916C is a long GRB. The PSD index values for b0, n3, n4 detectors are -1.8091, -2.2876, -2.0103 respectively and this implies the existence of pink and red noise in the data signal of this GRB. The constant noise floor level values are obtained as -1.5653, -2.7931, -2.6991 respectively. The data upto this level can only be used to study the variability of GRB080916C.

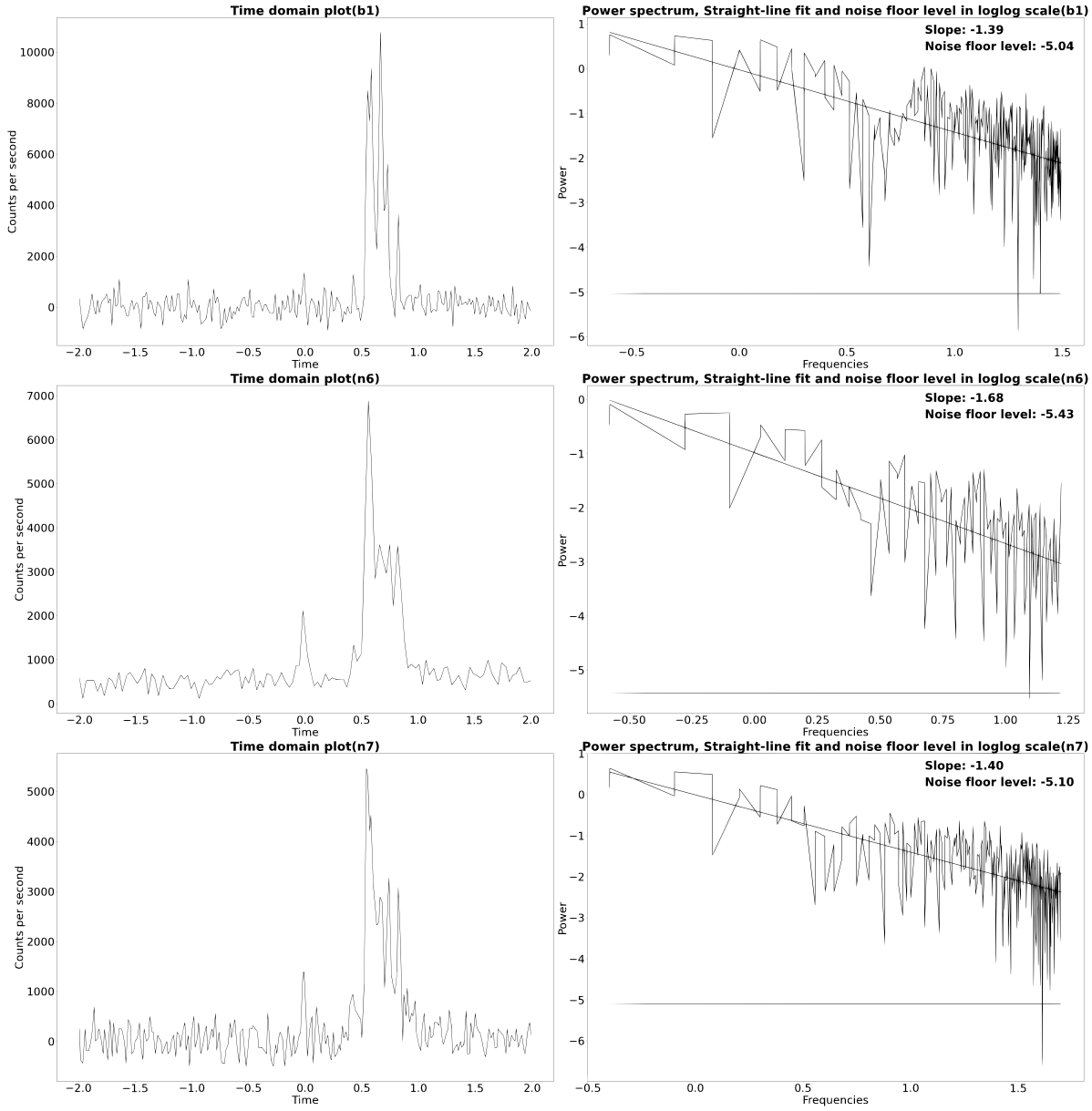

Figure 4.2: The multiple plot consisting of light curves and power spectra of data obtained from three detectors for the GRB090510. The data from one BGO b1 detector and two NaI detectors n6 and n7(16 ms binning time for all these detectors are chosen for plotting a more detailed LC) are used for the analysis of this GRB. The trigger time for all these detectors were from -2 to 10 seconds. The burst time was observed to be between -2 and 2 seconds and here LC and PSD are obtained for that time. Based on this burst time it is evident that the GRB090510 is a short GRB. The PSD index values for b1, n6, n7 detectors are -1.3947, -1.6793, -1.3954 respectively and this implies the existence of pink noise domination in the data signal of this GRB. The constant noise floor level values are obtained as -5.0350, -5.4307, -5.0970 respectively. The data upto this level can only be used to study the variability of GRB090510.

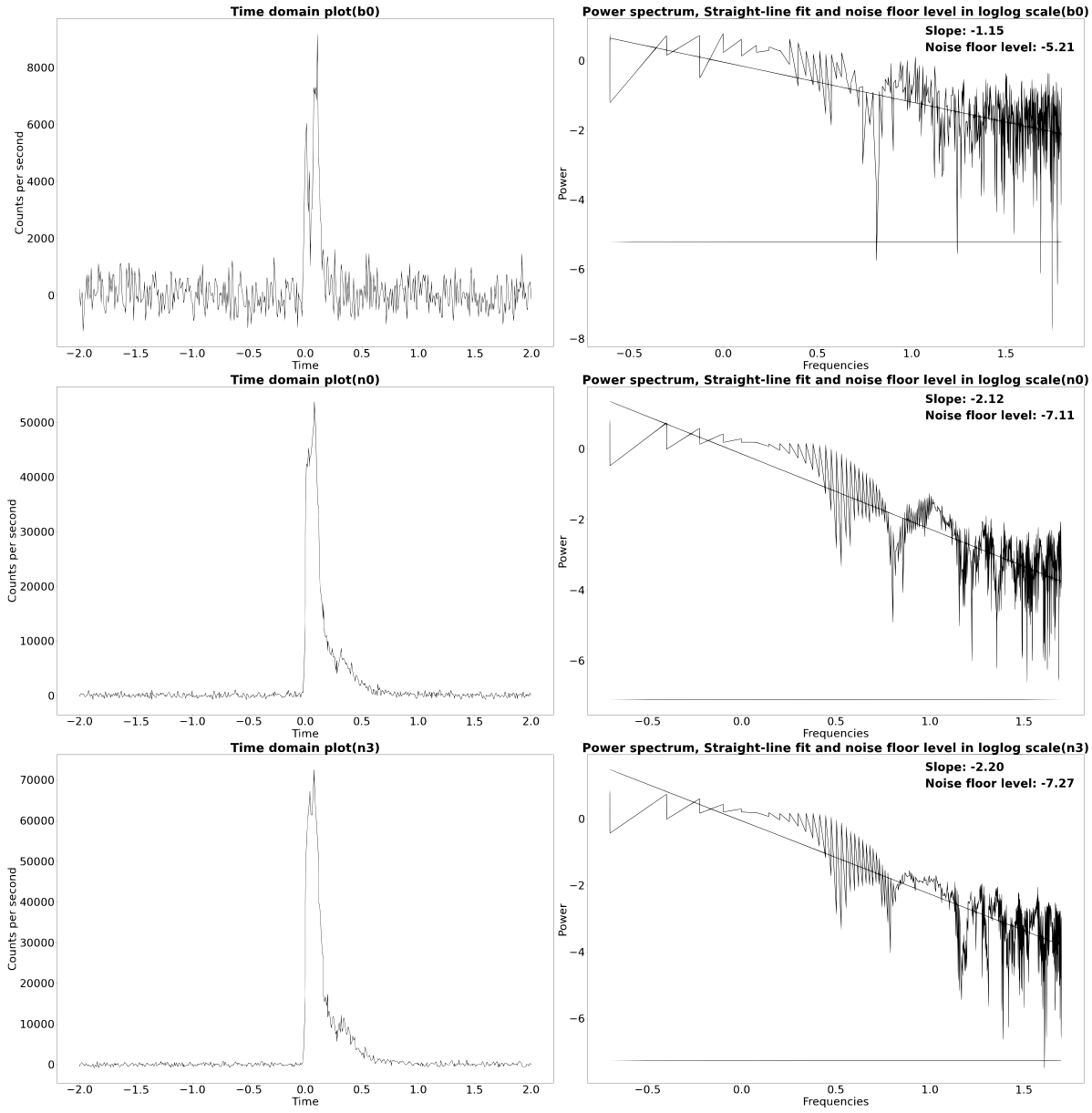

Figure 4.3: The multiple plot consisting of light curves and power spectra of data obtained from three detectors for the GRB120323A. The data from one BGO b0 detector and two NaI detectors n0 and n3(8 ms binning time is used in this case) are used for the analysis of this GRB. The trigger time for all these detectors were from -2 to 10 seconds. The burst time was observed to be between -2 and 2 seconds and here LC and PSD are obtained for that time. Based on this burst time it is evident that the GRB120323A is a short GRB. The PSD index values for b0, n0, n3 detectors are -1.1489, -2.1234, -2.1996 respectively and this implies the existence of pink and red noise in the data signal of this GRB. The constant noise floor level values are obtained as -5.2110, -7.1082, -7.2720 respectively. The data upto this level can only be used to study the variability of GRB120323A.

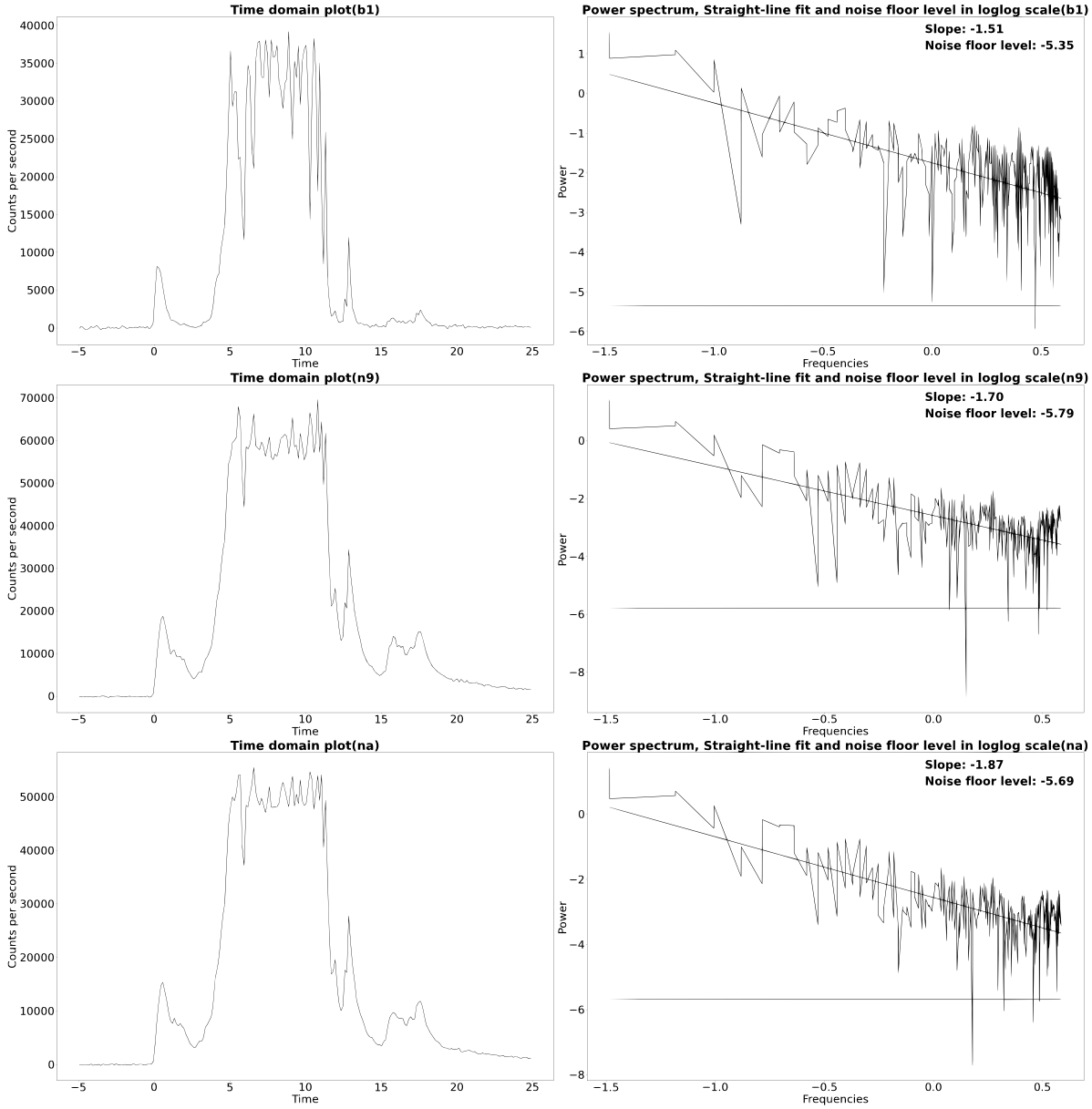

Figure 4.4: The multiple plot consisting of light curves and power spectra of data obtained from three detectors for the GRB130427A. The data from one BGO b1(binning time chosen for this detector is 128 ms) detector and two NaI detectors n9 and na are used for the analysis of this GRB. The trigger time for all these detectors were from -5 to 150 seconds. The burst time was observed to be between -5 and 25 seconds and here LC and PSD are obtained for that time. Based on this burst time it is evident that the GRB130427A is a long GRB. The PSD index values for b1, n9, na detectors are -1.5108, -1.6987, -1.8664 respectively and this implies the existence of pink noise in the data signal of this GRB. The constant noise floor level values are obtained as -5.3499, -5.7871, -5.6919 respectively. The data upto this level can only be used to study the variability of GRB130427A.

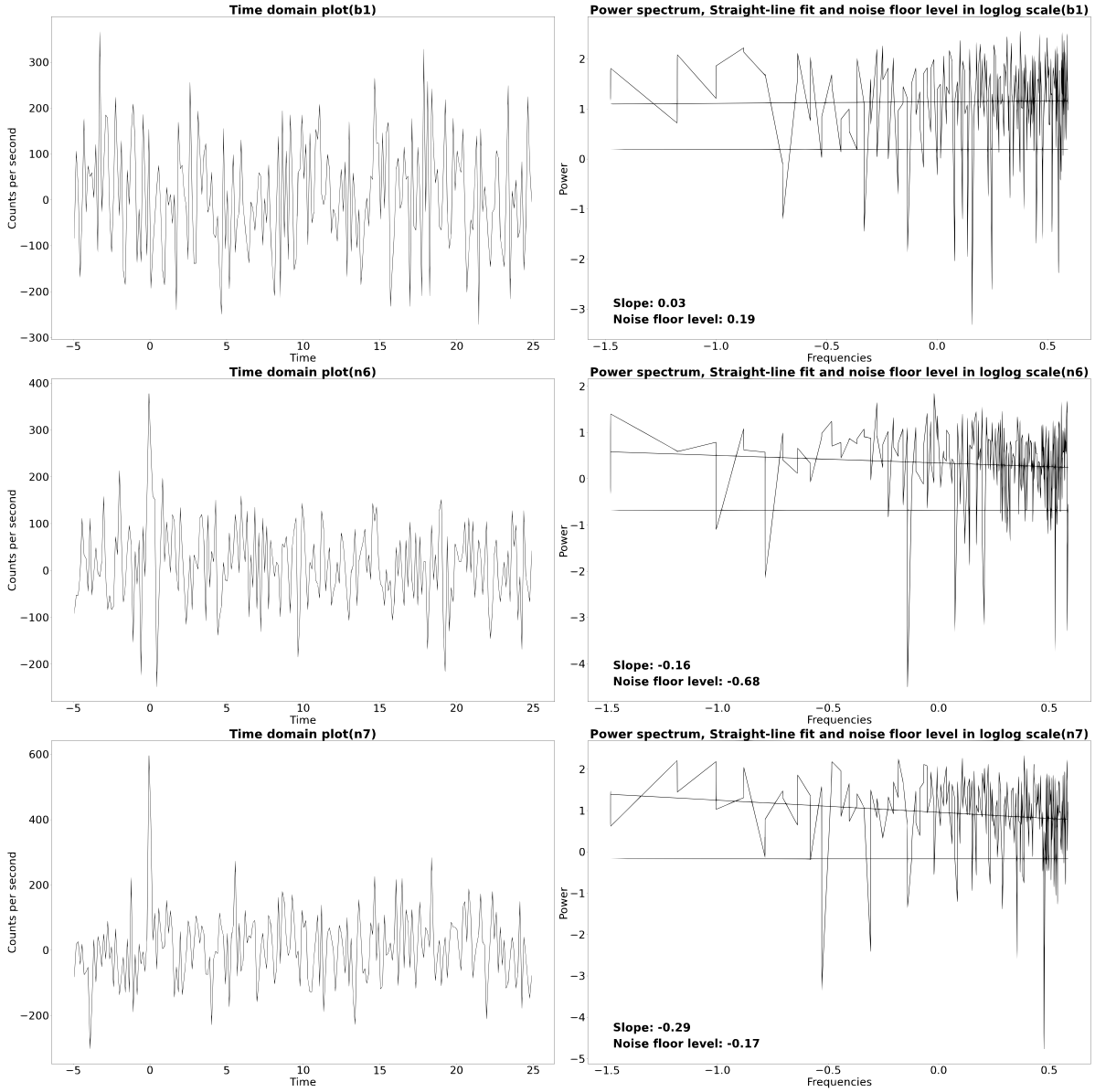

Figure 4.5: The multiple plot consisting of light curves and power spectra of data obtained from three detectors for the GRB150101B. The data from one BGO b1 detector and two NaI detectors n6 and n7 are used for the analysis of this GRB. The trigger time for all these detectors were from -5 to 25 seconds. The burst time was observed to be between -5 and 25 seconds and here LC and PSD are obtained for that time. Based on this burst time it is evident that the GRB150101B is a short GRB. The PSD index values for b1, n6, n7 detectors are 0.0305, -0.1620, -0.2944 respectively and this implies the existence of white noise in the data signal of this GRB. The constant noise floor level values are obtained as 0.1862, -0.6821, -0.1719 respectively. The data upto this level can only be used to study the variability of GRB150101B.

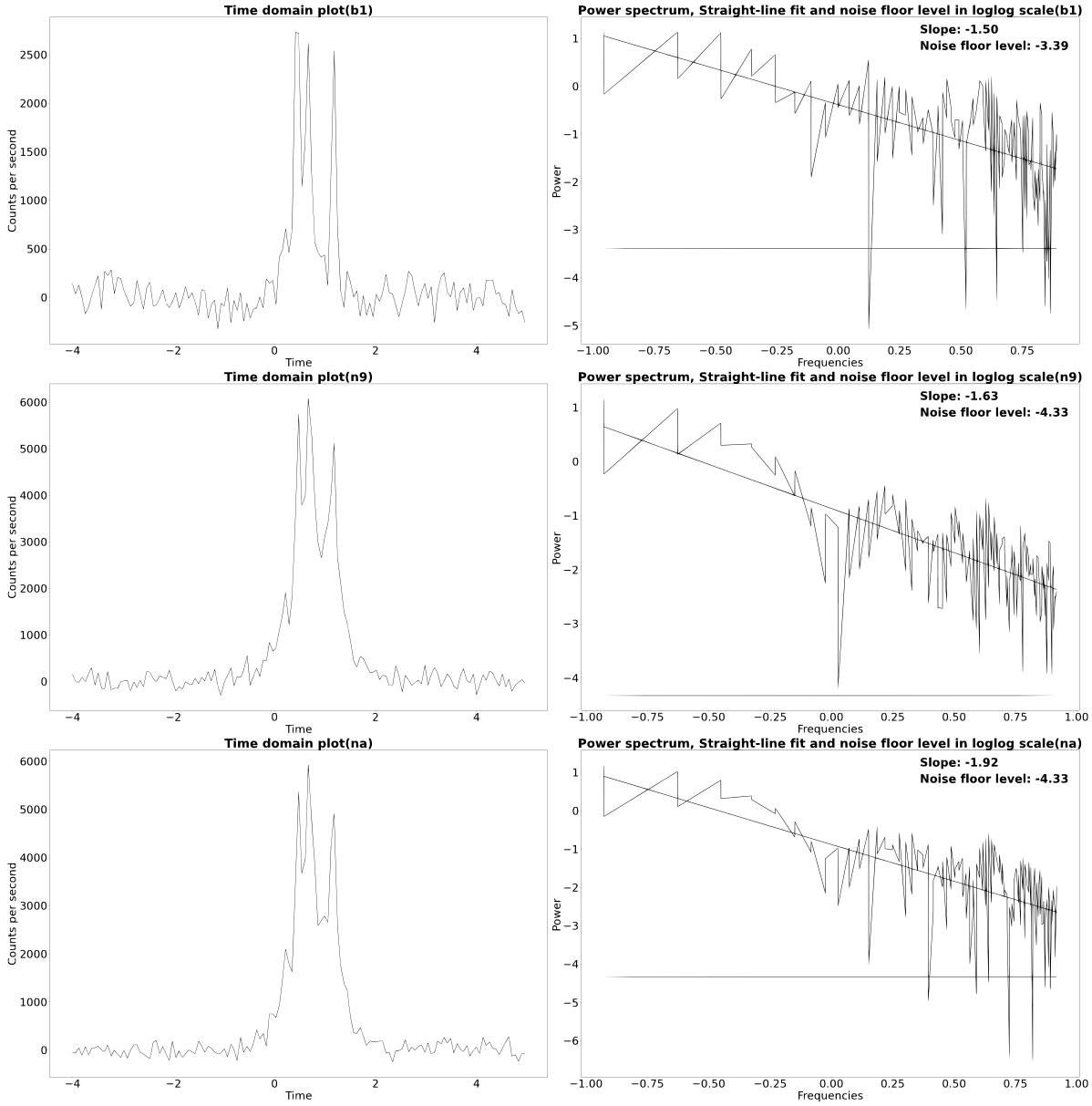

Figure 4.6: The multiple plot consisting of light curves and power spectra of data obtained from three detectors for the GRB170206A. The data from one BGO b1 detector and two NaI detectors n9 and na are used for the analysis of this GRB. The trigger time for all these detectors were from -4 to 20 seconds. The burst time was observed to be between -4 and 5 seconds and here LC and PSD are obtained for that time. Based on this burst time it is evident that the GRB170206A is a short GRB. The PSD index values for b1, n9, na detectors are -1.5039, -1.6315, -1.9185 respectively and this implies the existence of pink noise in the data signal of this GRB. The constant noise floor level values are obtained as -3.3924, -4.3303, -4.3291 respectively. The data upto this level can only be used to study the variability of GRB170206A.

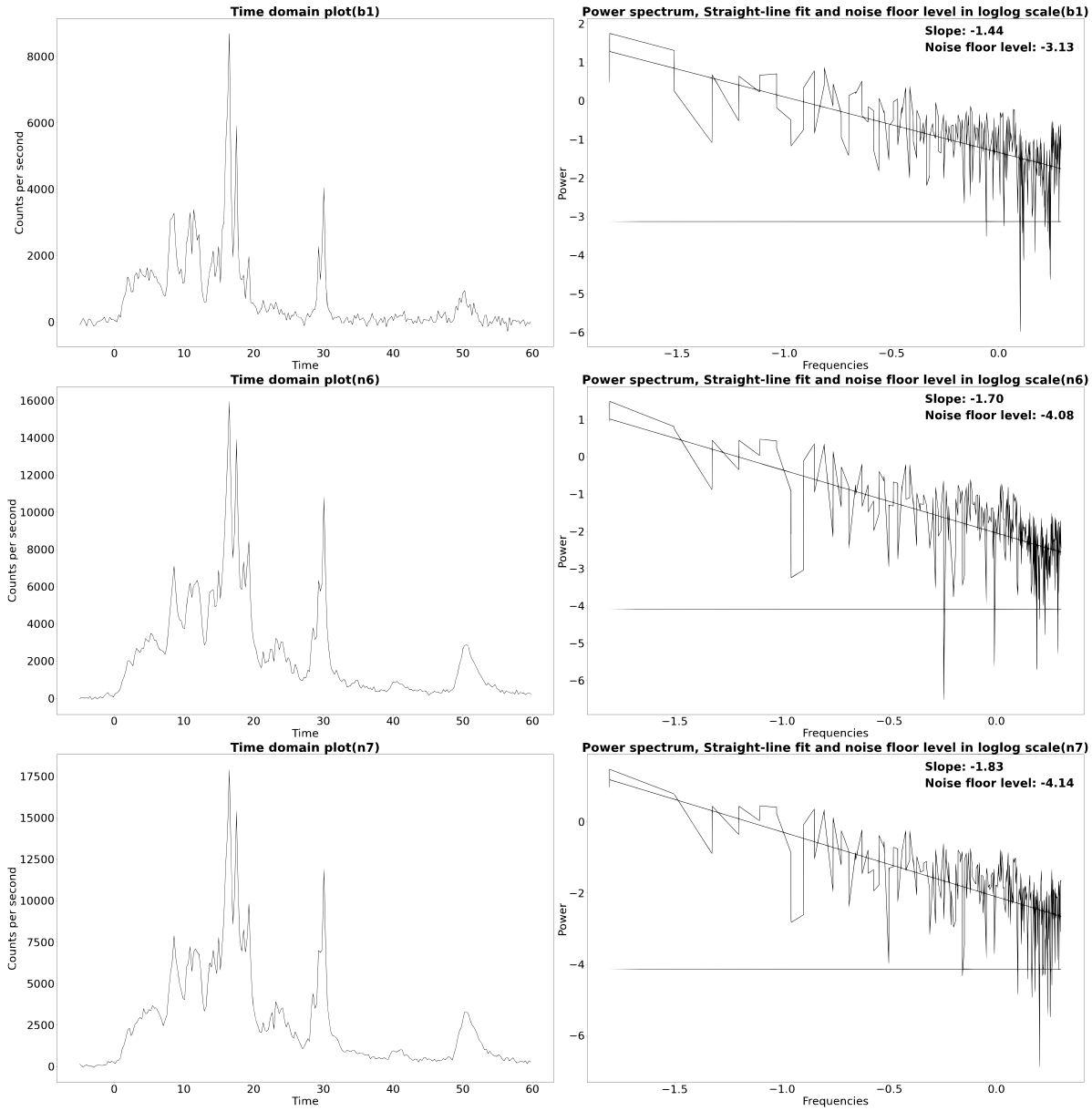

Figure 4.7: The multiple plot consisting of light curves and power spectra of data obtained from three detectors for the GRB180720B. The data from one BGO b1 detector and two NaI detectors n6 and n7(256 ms binning time of data is used for all three detectors in this GRB) are used for the analysis of this GRB. The trigger time for all these detectors were from -5 to 120 seconds. The burst time was observed to be between -5 and 60 seconds and here LC and PSD are obtained for that time. Based on this burst time it is evident that the GRB180720B is a long GRB. The PSD index values for b1, n6, n7 detectors are -1.4425, -1.6965, -1.8252 respectively and this implies the existence of pink noise in the data signal of this GRB. The constant noise floor level values are obtained as -3.1311, -4.0837, -4.1404 respectively. The data upto this level can only be used to study the variability of GRB180720B.

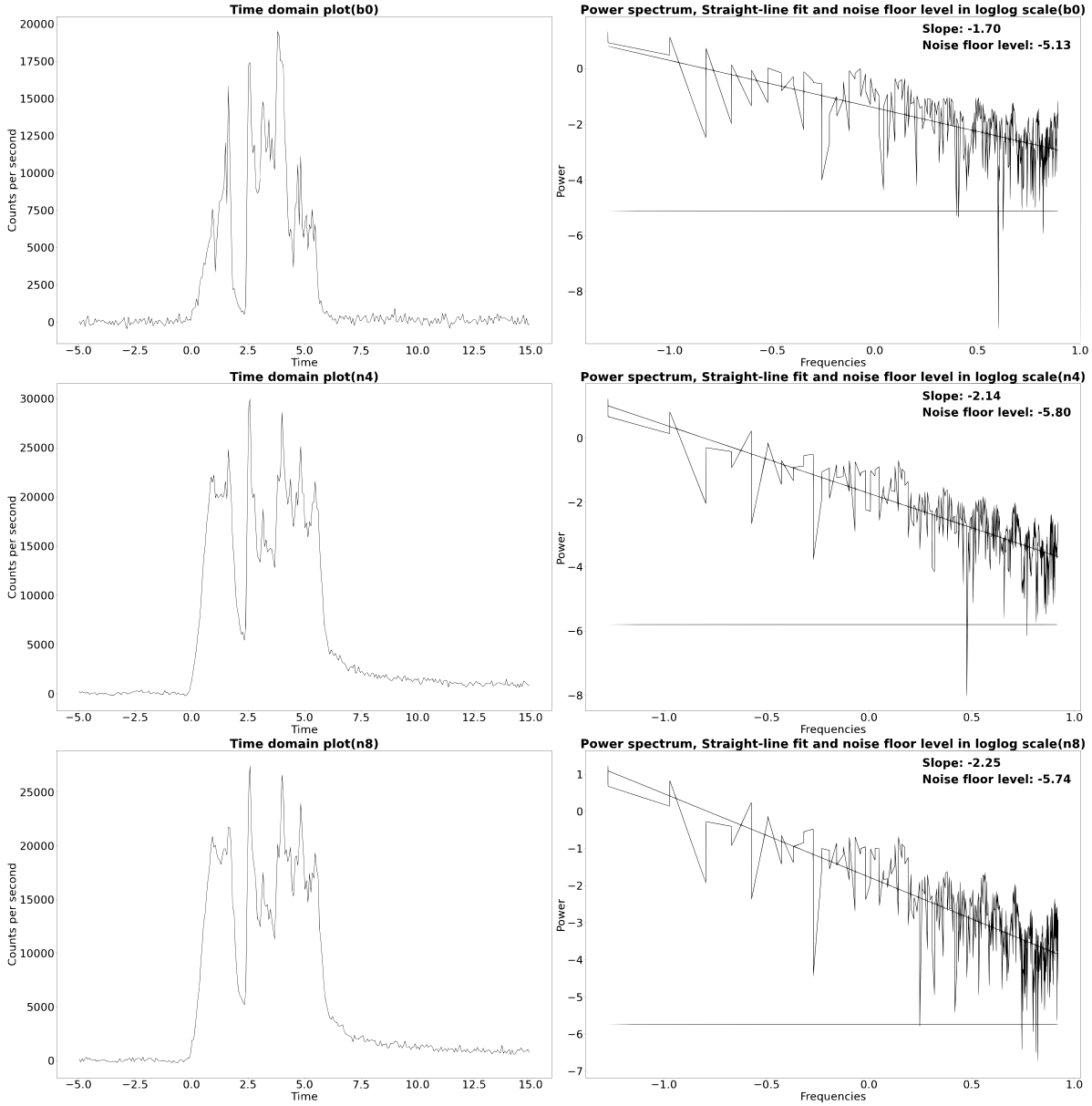

Figure 4.8: The multiple plot consisting of light curves and power spectra of data obtained from three detectors for the GRB190114C. The data from one BGO b0 detector and two NaI detectors n4 and n8 are used for the analysis of this GRB. The trigger time for all these detectors were from -5 to 120 seconds. The burst time was observed to be between -5 and 15 seconds and here LC and PSD are obtained for that time. Based on this burst time it is evident that the GRB190114C is a long GRB. The PSD index values for b0, n4, n8 detectors are -1.7012, -2.1409, -2.2515 respectively and this implies the existence of pink and red noise in the data signal of this GRB. The constant noise floor level values are obtained as -5.1252, -5.8005, -5.7404 respectively. The data upto this level can only be used to study the variability of GRB190114C.

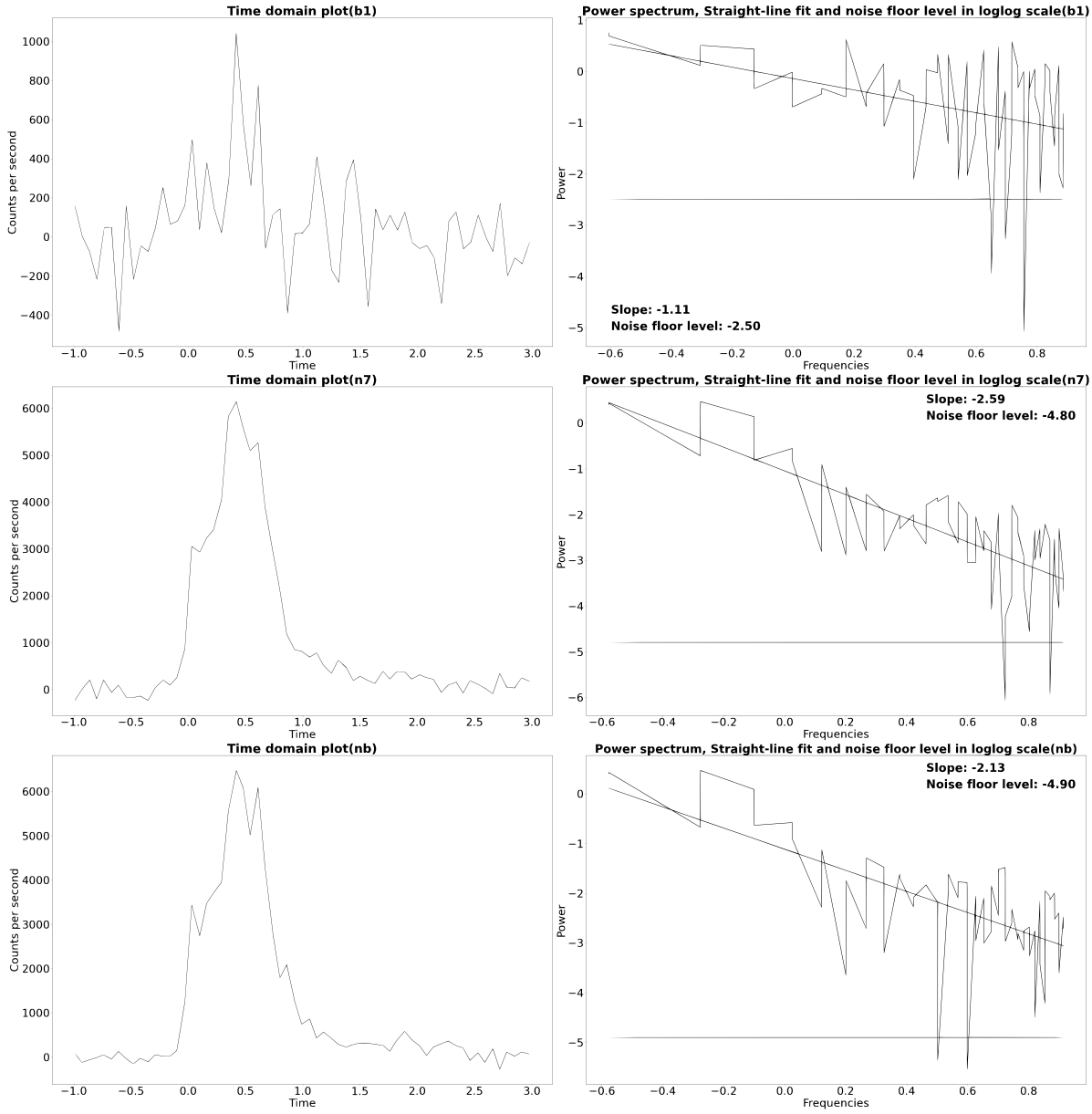

Figure 4.9: The multiple plot consisting of light curves and power spectra of data obtained from three detectors for the GRB200826A. The data from one BGO b1(the data for which the binning time is 64 ms is chosen) detector and two NaI detectors n7 and nb are used for the analysis of this GRB. The trigger time for all these detectors were from -4 to 25 seconds. The burst time was observed to be between -1 and 3 seconds and here LC and PSD are obtained for that time. Based on this burst time it is evident that the GRB200826A is a short GRB. The PSD index values for b1, n7, nb detectors are -1.1113, -2.5901, -2.1259 respectively and this implies the existence of pink and red noise in the data signal of this GRB. The constant noise floor level values are obtained as -2.4951, -4.7982, -4.9035 respectively. The data upto this level can only be used to study the variability of GRB200826A.

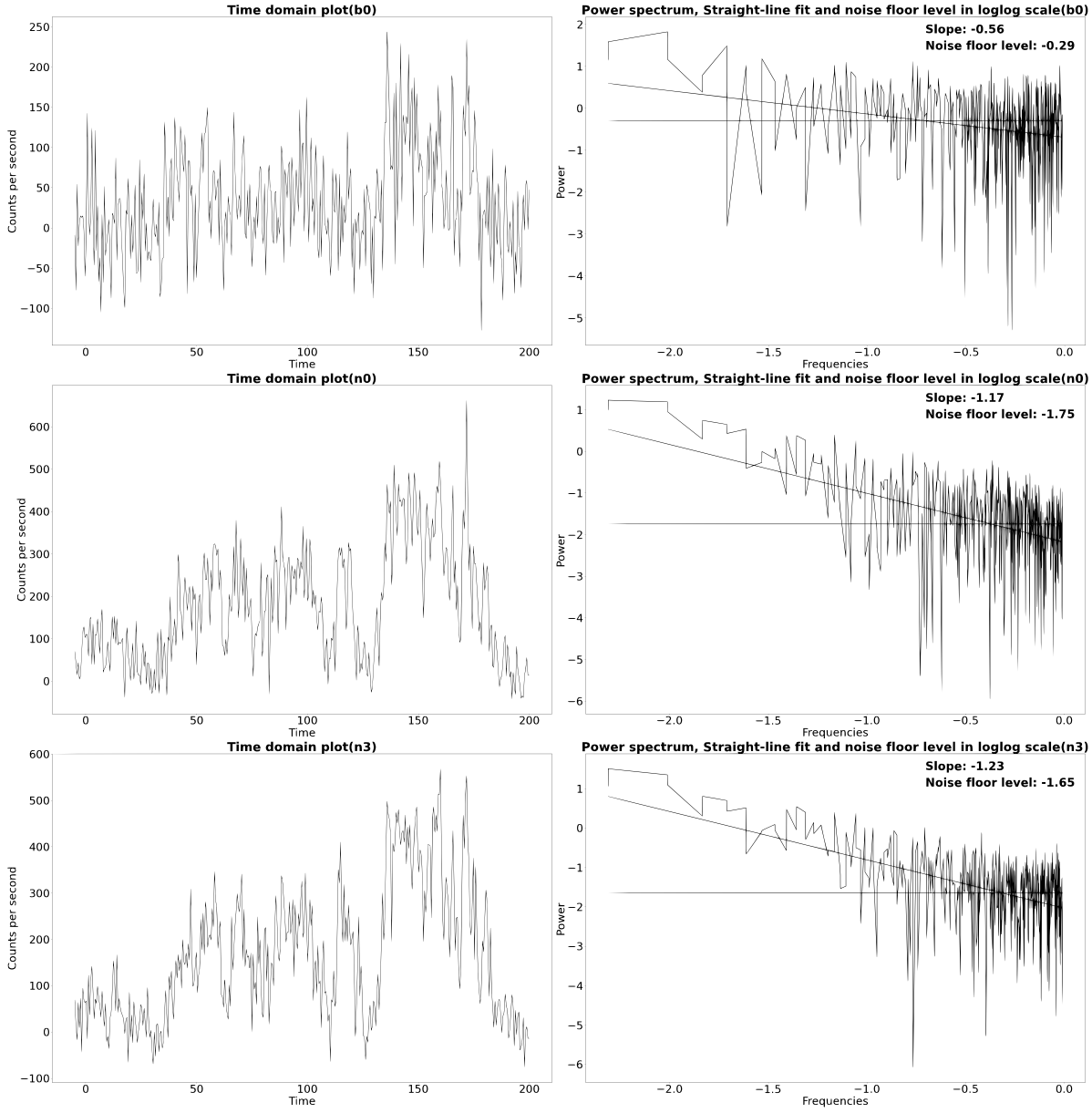

Figure 4.10: The multiple plot consisting of light curves and power spectra of data obtained from three detectors for the GRB220627A. The data from one BGO b0 detector and two NaI detectors n0 and n3(data with binning time 512 ms s chosen for all three detectors) are used for the analysis of this GRB. The trigger time for all these detectors were from -5 to 200 seconds. The burst time was observed to be between -5 and 200 seconds and here LC and PSD are obtained for that time. Based on this burst time it is evident that the GRB220627A is a long GRB. The PSD index values for b0, n0, n3 detectors are -0.5552, -1.1735, -1.2276 respectively and this implies the existence of white and pink noise in the data signal of this GRB. The constant noise floor level values are obtained as -0.2936, -1.7452, -1.6455 respectively. The data upto this level can only be used to study the variability of GRB220627A.

No.	GRB	X-axis limit	Detector	PL index	Noise floor level
1	080916C	[-5, 25]	b0	-1.81	-1.57
			n3	-2.29	-2.79
			n4	-2.01	-2.70
2	090510	[-2, 2]	b1(16 ms)	-1.39	-5.04
			n6(16 ms)	-1.68	-5.43
			n7(16 ms)	-1.40	-5.10
3	120323A	[-2, 2]	b0(8 ms)	-1.15	-5.21
			n0	-2.12	-7.11
			n3	-2.20	-7.27
4	130427A	[-5, 25]	b1(128 ms)	-1.51	-5.35
			n9	-1.70	-5.79
			na	-1.87	-5.69
5	150101B	[-5, 25]	b1	0.03	0.19
			n6	-0.16	-0.68
			n7	-0.29	-0.17
6	170206A	[-4, 5]	b1	-1.50	-3.39
			n9	-1.63	-4.33
			na	-1.92	-4.33
7	180720B	[-5, 60]	b1(256 ms)	-1.44	-3.13
			n6(256 ms)	-1.70	-4.08
			n7(256 ms)	-1.83	-4.14
8	190114C	[-5, 15]	b0	-1.70	-5.13
			n4	-2.14	-5.80
			n8	-2.25	-5.74
9	200826A	[-1, 3]	b1(64 ms)	-1.11	-2.50
			n7	-2.59	-4.80
			nb	-2.13	-4.90
10	220627A	[-5, 200]	b0(512 ms)	-0.56	-0.29
			n0(512 ms)	-1.17	-1.75
			n3(512 ms)	-1.23	-1.65

Table 4.1: Power-law index and noise floor level values of 10 GRBs which are detected by the Gamma-ray Burst Monitor detectors.

Chapter 5

Conclusions and future works

The GRB prompt emission data from GBM detectors of the Fermi telescope was obtained for a sample of 10 GRBs and used to plot their corresponding light curves and Power Density Spectra. The variability exhibited by each GRB can be understood by Fast Fourier Transform. Their PDSs are fitted and well-represented by a power-law model. The power spectral analysis was done for different energy bands. Our results indicate that GRBs show energy-dependent variability. The PSD obtained at different energies from BGO and NaI detectors indicate different power-law slopes. The noise floor levels were also computed and marked in the same PSD curves.

However, it was observed from our analysis, with the data of a few GRBs, that no significant differences have been found between the slopes and the power spectra of short and long GRBs. We have developed an analysis tool for obtaining PSDs in the project. I wish to extend this work to many GRBs to study their variability using PSD in the future. Future studies on the variability of the GRB light curve may shed light on the two classes of GRBs and their environment.

Bibliography

1. Brault, J. & White, O. The analysis and restoration of astronomical data via the fast Fourier transform. *Astronomy and Astrophysics* **13,** 169 (1971)
2. Beloborodov, A. M., Stern, B. E. & Svensson, R. Power density spectra of gamma-ray bursts. *The Astrophysical Journal* **535,** 158 (2000). doi: https://doi.org/10.1086/308836
3. Lloyd, N. M. & Petrosian, V. Synchrotron radiation as the source of gamma-ray burst spectra. *The Astrophysical Journal* **543,** 722 (2000). doi:10.1086/317125
4. Piran, T. The physics of gamma-ray bursts. *Reviews of Modern Physics* **76,** 1143 (2005). doi:https://doi.org/10.48550/arXiv.astro-ph/0405503
5. Ghirlanda, G., Nava, L., Ghisellini, G., Celotti, A. & Firmani, C. Short versus long gamma-ray bursts: spectra, energetics, and luminosities. *Astronomy & Astrophysics* **496,** 585–595 (2009). doi:https://doi.org/10.1016/j.jheap.2015.07.002
6. Meegan, C. *et al.* The Fermi gamma-ray burst monitor. *The Astrophysical Journal* **702,** 791 (2009). doi:https://doi.org/10.1016/j.physrep.2014.09.008
7. Kouveliotou, C., Wijers, R. A. & Woosley, S. *Gamma-ray Bursts* (Cambridge University Press, 2012)
8. Sastry, S. S. *Introductory methods of numerical analysis* (PHI Learning Pvt. Ltd., 2012)
9. Bissaldi, E., Peretti, E. & Longo, F. Temporal properties of bright BGO GRBs detected by Fermi. *arXiv preprint arXiv:1502.04714* (2015). doi:https://doi.org/10.48550/arXiv.1502.04714
10. D'Avanzo, P. Short gamma-ray bursts: A review. *Journal of High Energy Astrophysics* **7,** 73–80 (2015). doi:https://doi.org/10.1016/j.jheap.2015.07.002
11. Ghirlanda, G., Bernardini, M. G., Calderone, G. & D'Avanzo, P. Are short Gamma Ray Bursts similar to long ones? *Journal of High Energy Astrophysics* **7,** 81–89 (2015). doi:https://doi.org/10.1016/j.jheap.2015.04.002
12. Kumar, P. & Zhang, B. The physics of gamma-ray bursts & relativistic jets. *Physics Reports* **561,** 1–109 (2015). doi:https://doi.org/10.1016/j.physrep.2014.09.008
13. Wang, K., Liu, R.-Y., Dai, Z.-G. & Asano, K. Hadronic origin of prompt high-energy emission of gamma-ray bursts revisited: in the case of a limited maximum proton energy. *The Astrophysical Journal* **857,** 24 (2018). doi: 10.3847/1538-4357/aab667
14. Zhang, B. *The physics of gamma-ray bursts* (Cambridge University Press, 2018). doi:10.1017/97811392

15. Zhang, Y., Geng, J.-J. & Huang, Y.-F. Inverse Compton Scattering Spectra of gamma-ray burst prompt emission. *The Astrophysical Journal* **877,** 89 (2019). doi: 10.3847/1538-4357/ab1b10

16. Coppin, P., de Vries, K. D. & van Eijndhoven, N. Identification of gamma-ray burst precursors in Fermi-GBM bursts. *Physical Review D* **102,** 103014 (2020). doi: https://doi.org/10.1103/Ph

17. Goyal, A. Optical variability power spectrum analysis of blazar sources on intranight timescales. *The Astrophysical Journal* **909,** 39 (2021). doi: https://doi.org/10.3847/1538-4357/abd7fb

18. Tarnopolski, M. & Marchenko, V. A Comprehensive Power Spectral Density Analysis of Astronomical Time Series. II. The Swift/BAT Long Gamma-Ray Bursts. *The Astrophysical Journal* **911,** 20 (2021). doi:https://doi.org/10.3847/1538-4357/abe5b1

19. Miceli, D. & Nava, L. Gamma-Ray Bursts Afterglow Physics and the VHE Domain. *Galaxies* **10,** 66 (2022). doi:https://doi.org/10.48550/arXiv.2205.12146

20. Thompson, D. J. & Wilson-Hodge, C. A. Fermi Gamma-ray Space Telescope. *arXiv preprint arXiv:2210.12875* (2022). doi:https://doi.org/10.48550/arXiv.2210.12875

21. Ursi, A. *et al.* The Second AGILE MCAL Gamma-Ray Burst Catalog: 13 yr of Observations. *The Astrophysical Journal* **925,** 152 (2022). doi:http://dx.doi.org/10.3847/1538-4357/ac3df7

9% Overall Similarity

Top sources found in the following databases:

- 7% Internet database
- Crossref database
- 5% Submitted Works database
- 7% Publications database
- Crossref Posted Content database

TOP SOURCES

The sources with the highest number of matches within the submission. Overlapping sources will not be displayed.

1	**arxiv.org** Internet	2%
2	**David J. Thompson, Colleen A. Wilson-Hodge. "Chapter 58-1 Fermi Ga...** Crossref	1%
3	**Tsvi Piran. "The physics of gamma-ray bursts", Reviews of Modern Phy...** Crossref	<1%
4	**iopscience.iop.org** Internet	<1%
5	**mpi-hd.mpg.de** Internet	<1%
6	**um.edu.mt** Internet	<1%
7	**ia802907.us.archive.org** Internet	<1%
8	**University of Crete on 2022-10-31** Submitted works	<1%

9	Anna Y. Q. Ho. "The Landscape of Relativistic Stellar Explosions", Sprin... Crossref	<1%
10	mdpi-res.com Internet	<1%
11	tel.archives-ouvertes.fr Internet	<1%
12	koreascience.or.kr Internet	<1%
13	Calamvale Community College on 2021-08-11 Submitted works	<1%
14	University of Hertfordshire on 2022-12-19 Submitted works	<1%
15	cds.cern.ch Internet	<1%
16	Syed Ali Mohsin Bukhari, Saeeda Sajjad, Urooj Murtaza. "The spectral a... Crossref	<1%
17	Angela Zegarelli. "Detection prospects for multi-GeV neutrinos from co... Crossref	<1%
18	M. De Pasquale. "A Comparative Study of the X-Ray Afterglow Properti... Crossref	<1%
19	opus4.kobv.de Internet	<1%
20	Liverpool John Moores University on 2022-12-08 Submitted works	<1%

21	Paul Coppin, Krijn D. de Vries, Nick van Eijndhoven. "Identification of g... Crossref	<1%
22	open.library.ubc.ca Internet	<1%
23	Visvesvaraya Technological University on 2014-11-05 Submitted works	<1%
24	spiedigitallibrary.org Internet	<1%
25	veritas.sao.arizona.edu Internet	<1%
26	ba.infn.it Internet	<1%
27	University of Crete on 2022-11-13 Submitted works	<1%
28	personale.unimore.it Internet	<1%
29	P. D'Avanzo, R. Salvaterra, M. G. Bernardini, L. Nava, S. Campana, S. Co... Crossref	<1%
30	ujcontent.uj.ac.za Internet	<1%
31	Kai Wang, Ruo-Yu Liu, Zi-Gao Dai, Katsuaki Asano. "Hadronic Origin of ... Crossref	<1%
32	S Dichiara, E Troja, V Lipunov, R Ricci et al. "The early afterglow of GRB... Crossref	<1%

33	Thompson, David J.. "Space detectors for gamma rays (100 MeV-100 ... Crossref	<1%
34	ruj.uj.edu.pl Internet	<1%
35	dcgi.fel.cvut.cz Internet	<1%
36	iihe.ac.be Internet	<1%
37	arxiv-vanity.com Internet	<1%
38	researchgate.net Internet	<1%
39	Zeinab Kalantari, Alaa Ibrahim, Mohammad Reza Rahimi Tabar, Sohrab... Crossref	<1%
40	doi.org Internet	<1%
41	intechopen.com Internet	<1%
42	mdpi.com Internet	<1%
43	science.gov Internet	<1%

Excluded from Similarity Report

- Bibliographic material
- Cited material
- Manually excluded text blocks
- Quoted material
- Small Matches (Less then 12 words)

EXCLUDED TEXT BLOCKS

Manesh MichaelAssistant Professor, Department of Physics,Bharata Mata College...

web.iucaa.in

in partial

Visvesvaraya Technological University on 2014-10-28

for the

BMS College of Engineering on 2022-06-30

by me and submitted in partial

Visvesvaraya Technological University on 2014-11-05

declare that the

www.coursehero.com

will bethe property of

www.coursehero.com

of Astronomy, Astrophysics and Space Engineering(DAASE

timesofindia.indiatimes.com

1 Introduction

hdl.handle.net

2.1 Short Gamma Ray Bursts 2.2

en.wikipedia.org

3.1

Indian Institute of Technology Jodhpur on 2021-02-03

3.2.2Fast Fourier Transform(FFT) 3.2.3

www.budde.com.au

4 Results and Discussion4.1 Light curves . . . .

aa.springer.de

to detect gamma

en.wikipedia.org

the Large Area Telescope(LAT) and the Gamma-RayBurst Monitor(GBM

www.science.gov

Gamma ray burstsGamma-ray bursts are highly energetic explosions

www.chegg.com

GRBsdetected by BATSE instrument

S. P. Plunkett, M. Delaney, B. McBreen, K. J. Hurley, C. T. O'Sullivan. "A search for ultra-high energy counterp...

2

University of Liverpool on 2023-03-23